HHS Public Access

Author manuscript

Cell Rep. Author manuscript; available in PMC 2023 December 12.

Published in final edited form as:

Cell Rep. 2023 October 31; 42(10): 113272. doi:10.1016/j.celrep.2023.113272.

Primary cilia control oligodendrocyte precursor cell proliferation in white matter injury via Hedgehog-independent CREB signaling

Kimberly K. Hoi[1], **Wenlong Xia**[1], **Ming Ming Wei**[1], **Maria Jose Ulloa Navas**[2], **Jose-Manuel Garcia Verdugo**[2], **Maxence V. Nachury**[3], **Jeremy F. Reiter**[4,5], **Stephen P.J. Fancy**[1,6,*]

[1]Departments of Neurology and Pediatrics, Division of Neuroimmunology and Glial Biology, Newborn Brain Research Institute, University of California, San Francisco, San Francisco, CA 94158, USA

[2]Laboratorio de Neurobiología Comparada, Instituto Cavanilles, Universidad de Valencia, CIBERNED, 46980 Paterna, Spain

[3]Department of Ophthalmology, University of California, San Francisco, San Francisco, CA 94143, USA

[4]Department of Biochemistry and Biophysics, Cardiovascular Research Institute, University of California, San Francisco, San Francisco, CA 94158, USA

[5]Chan Zuckerberg Biohub, San Francisco, CA 94158, USA

[6]Lead contact

SUMMARY

Remyelination after white matter injury (WMI) often fails in diseases such as multiple sclerosis because of improper recruitment and repopulation of oligodendrocyte precursor cells (OPCs) in lesions. How OPCs elicit specific intracellular programs in response to a chemically and mechanically diverse environment to properly regenerate myelin remains unclear. OPCs construct primary cilia, specialized signaling compartments that transduce Hedgehog (Hh) and G-protein-coupled receptor (GPCR) signals. We investigated the role of primary cilia in the OPC response to WMI. Removing cilia from OPCs genetically via deletion of Ift88 results in OPCs failing to repopulate WMI lesions because of reduced proliferation. Interestingly, loss of cilia does not affect Hh signaling in OPCs or their responsiveness to Hh signals but instead leads to dysfunctional cyclic AMP (cAMP)-dependent cAMP response element-binding protein (CREB)-

*Correspondence: stephen.fancy@ucsf.edu.

AUTHOR CONTRIBUTIONS

K.K.H. and S.P.J.F. conceived and designed all experiments. K.K.H. performed experiments and analyzed data. W.X. and M.M.W. contributed to sample preparation, and M.J.U.N. and J.-M.G.V. contributed to electron microscopy for Figure 1B. J.F.R. contributed to analysis of RNA-seq data. M.V.N. and J.F.R. contributed to discussions. K.K.H. and S.P.J.F. wrote and edited the manuscript.

DECLARATION OF INTERESTS

The authors declare no competing interests.

SUPPLEMENTAL INFORMATION

Supplemental information can be found online at https://doi.org/10.1016/j.celrep.2023.113272.

mediated transcription. Because inhibition of CREB activity in OPCs reduces proliferation, we propose that a GPCR/cAMP/CREB signaling axis initiated at OPC cilia orchestrates OPC proliferation during development and in response to WMI.

In brief

Hoi et al. find that deletion of Ift88 in OPCs leads to loss of their primary cilia. OPCs require these cilia for proliferation in development and white matter injury. It is not required for canonical Hh signaling, and they propose that a primary cilium-initiated GPCR/cAMP/CREB signaling axis orchestrates OPC proliferation.

Graphical Abstract

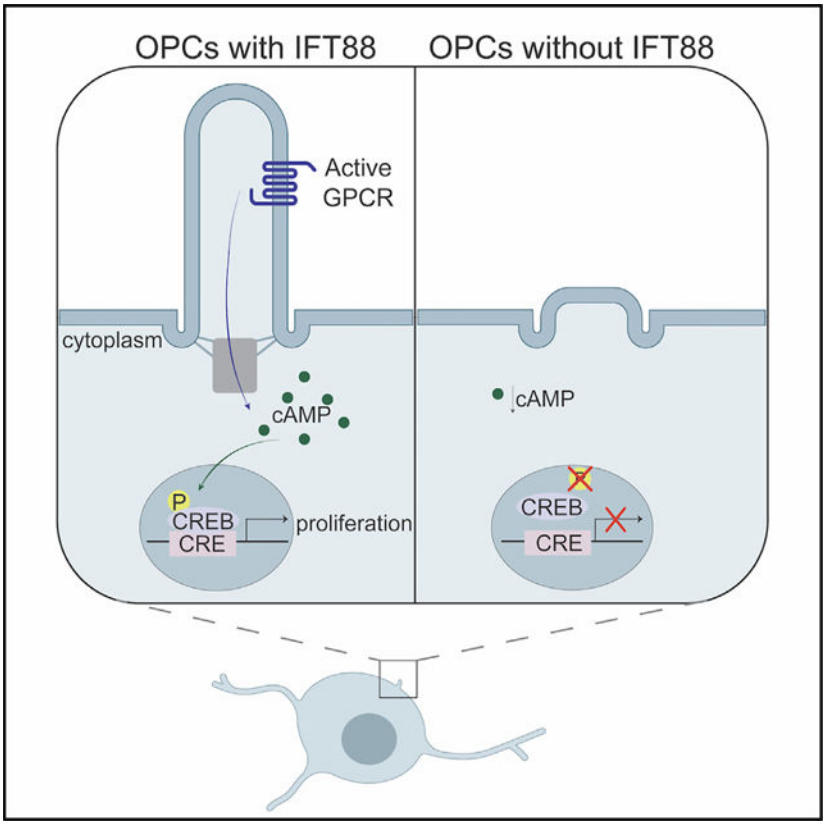

INTRODUCTION

Damage to axons and myelinating oligodendrocytes (OL) in white matter injury is an important component of multiple sclerosis (MS) in adults as well as newborn brain injuries that cause cerebral palsy and cognitive disabilities. Damaged myelin sheaths can be regenerated in both conditions, but human myelin repair is highly susceptible to failure. Successful remyelination and functional recovery of axons depends on adequate OL precursor cell (OPC) recruitment into lesions,[1,2] involving their significant proliferation in response to injury. Indeed, OPC depletion and inadequate recruitment are hallmarks of many chronically demyelinated lesions.[3,4] CNS developmental myelination also requires

that OPCs proliferate, migrate, and decide either to differentiate or remain a precursor in the appropriate spatiotemporal manner.[4–6] Mechanisms regulating OL development have been studied extensively, resulting in the identification of intrinsic and extrinsic factors that govern OPC migration, proliferation, and differentiation.[7] However, as OPCs do not reside in a well-defined niche because of their distribution and tiling,[8] it is unclear how OPCs are able to translate interactions with extracellular cues into specific intracellular responses in the context of the chemically and mechanically dense environments that exist in development and remyelination.

Signaling specificity is often achieved via the spatial compartmentalization of signaling pathway components. The primary cilium is a specialized signaling organelle that manifests as a slender protrusion of the cell membrane that is found on most vertebrate cells. The ciliary membrane surrounds an axoneme with a 9+0 microtubule arrangement that is separated from the rest of the cell body via a transition zone, establishing a ciliary compartment.[9] Proteins are transported bidirectionally along the ciliary axoneme through the conserved process of intraflagellar transport (IFT). IFT thus plays a crucial role in assembly and maintenance of the ciliary axoneme.[10–12] In partnership with IFT, ciliary anterograde and retrograde transport are mediated by kinesin II and the cytoplasmic dynein complex, respectively. Kinesin II, comprised of KIF3A, KIF3B, and KAP3, is crucial in the construction and maintenance of the primary cilium but also has critical extraciliary cytoskeletal roles and non-ciliary contributions to the regulation of Wnt signaling.[13–15]

Once thought of as vestigial organelles, primary cilia are now appreciated as specialized signaling organelles with critical roles in the transduction of mammalian Hedgehog (Hh)[16,17] and G-protein-coupled receptor (GPCR) signaling.[18,19] When Hh ligand binds to Ptch1, Smoothened (Smo) accumulates in the cilium resulting in the activation of Gli transcriptional effectors. In the absence of Hh, Gli transcription factors are processed into their repressor forms (GliR) to keep Hh signals off.[16] In support of this, disruption of ciliogenesis often results in phenotypes associated with the gain or loss of Hh.[20,21] Primary cilia have also been established as critical GPCR signaling centers,[22] with an expanding subset of GPCRs and their effector molecules localizing to cilia, including SSTR3[23,24] and GPR161.[25,26] Ligand binding results in the activation of heterotrimeric G-proteins to either stimulate or inhibit cyclic AMP production in the cell. Recently, it has been discovered that vertebrate cells are able to distinguish between ciliary and extraciliary GPCR signaling and cAMP,[27] providing further depth to the versatility and specificity of GPCR signaling.

Primary cilia have been described in OPCs *in vitro*[28] and in the adult mouse *in vivo.*[29,30] Deletion of Kif3a from OPCs in adult mice resulted in impaired proliferation in response to learning of a skilled motor task.[29] The function of cilia in white matter injury repair and signals transduced by OPC cilia remain poorly understood. Hh signaling is required for the specification of OPCs during embryonic development.[31,32] Studies involving the overexpression of sonic hedgehog (Shh) in the adult CNS suggest that oligodendroglial-lineage cells are responsive to Shh signals after focal demyelination.[33,34] Others report stage-specific Hh regulation of OLs during development, showing that continued expression of Smo in OPCs promotes proliferation while inhibiting differentiation.[35] Several GPCRs

have also been implicated in regulating OL development. Gpr17 intrinsically regulates OL differentiation and timing of myelination,[36] while Gpr56[37,38] regulates OPC proliferation.

We investigated the function of ciliary signaling in OPC development and white matter injury repair. Here we show that OPC cilia are required for and control proliferation during development and in response to focal demyelinating injury by regulating cAMP response element-binding protein (CREB)-mediated transcription but not Hh signaling.

RESULTS

OPCs are ciliated in mammalian CNS development and white matter injury

Previous studies indicate that OPCs are ciliated *in vitro* and in the adult mouse brain *in vivo*.[28,29] We sought to determine whether OPC cilia may be relevant to human white matter injury repair and found that human OPCs in this context are ciliated, shown as ARL13b-labeled primary cilia in $OLIG2^+$ cells from human neonatal hypoxic ischemic encephalopathy (HIE) (Figure 1A). To confirm the presence of cilia in OPCs morphologically, we performed electron microscopy in NG2-EGFP mice at post-natal day 60 (P60), where OPCs (which express NG2) are labeled with enhanced green fluorescent protein (EGFP), allowing identification of OPCs in electron micrographs via immunogold labeling. OPC cilia can be clearly seen on electron microscopy (EM), displaying the basal body, axoneme, and ciliary pockets (Figure 1B). We also confirm the presence of cilia on OPCs, but not mature OLs, in OPCs purified from P7 wild-type (WT) mice (Figure 1C).

To determine whether OPC ciliation changes throughout CNS development, we quantified the proportion of OPCs with cilia at different developmental time points. At embryonic day 13.5 (E13.5) in the developing mouse brain, 67.22% ± 3.67% OPCs are ciliated. This is reduced to 49.69% ± 4.71% at P0 and 35.21% ± 1.97% at P7 before stabilizing at 49.56% ± 0.75% and 48.56% ± 6.14% at P21 and P60, respectively (Figures 1D and 1E). The reduction of ciliated OPCs is likely due to proliferation and the previously characterized deconstruction of primary cilia as cells, including OPCs, enter the cell cycle.[39] Indeed, in the P7 cortex, cilia are present in only 9.58% of proliferating OPCs ($Ki67^+$) compared with 71.34% in non-dividing OPCs ($Ki67^-$) (Figure S1A). A similar trend was observed in the developing mouse spinal cord. At E13.5, 83.85% ± 8.61% of OPCs harbored cilia, which decreased to 35% ± 7.64% at P7 and increased to 41.03% ± 3.14% at P60 (Figures 1D and 1E). Similar to our results in purified OPCs, mature OLs in the P7 mouse cortex do not harbor primary cilia (Figure 1D), suggesting that cilia are deconstructed before or during differentiation.

We characterized OPC ciliation in white matter injury using an established lysolecithin-induced mouse model of demyelinating injury. We assessed lesions in the dorsal funiculus of the adult mouse spinal cord 5 day post lesion (5 dpl) and found that OPCs are also ciliated in mouse white matter injuries. In the white matter that surrounds the lesion core, 43.30% ± 1.68% of OPCs are ciliated, a proportion similar to what we observed in the uninjured P60 spinal cord. Within the demyelinated lesions, 19.08% ± 1.86% of OPCs harbor cilia (Figure 1F). The reduced percentage of ciliated OPCs within the lesion at 5 dpl reflects the well-characterized rapid proliferation of OPCs at this time point in this injury model.

Ciliogenesis is tightly coupled to the cell cycle, with deconstruction of the ciliary axoneme during cell division occurring to allow the centrosome to fulfill its role as a microtubule organizing center, followed by reconstruction of cilia after cell division.[39] The presence of ciliated OPCs within lesions indicates that OPCs can be responsive to signals transduced through cilia after white matter injury.

Removing cilia from OPCs decreases proliferation in development

To assess whether primary cilia function in oligodendroglial development, we removed cilia in OPCs by genetically deleting a critical component of ciliary maintenance. Deletion of components involved in IFT, such as Ift88, results in disrupted ciliogenesis, effective loss of primary cilia, and loss of ciliary signaling. We generated PDGFRα-Cre: $Ift88^{fl/fl}$; RosaEYFP mice (called Ift88 cKO (conditional knockout) hereafter), in which OPCs with Ift88 conditionally deleted express enhanced yellow fluorescent protein (EYFP) (labeled with GFP). Littermates expressing PDGFRα-Cre and possessing a WT Ift88 allele (PDGFRα-Cre: $Ift88^{fl/wt}$; RosaEYFP) served as controls. We used EYFP to verify that recombination in these mice occurs in OPCs expressing Pdgfrα (Figure 2A; Figure S1D). Conditional removal of Ift88 from $EYFP^+$ cells caused Ift88 and cilium loss, resulting in a 90% reduction in ciliated $EYFP^+$ oligodendroglia ($EYFP^+Arl13b^+$) (Figure 2B; Figures S1B and S1C).

By P7, OPCs are well distributed across the mouse brain in WT mice and have begun to differentiate in the white matter but are still highly proliferative in the cortex. Ift88 cKO mice, however, exhibited a marked 40% reduction in the density of $EYFP^+$ oligodendroglia compared with controls in the P7 cortex (Figure 2C). Despite this, the number of total $Pdgfr\alpha^+$ OPCs in the P7 Ift88 cKO cortex remained unchanged compared with controls. This was due to a compensatory increase in the proliferation of $EYFP^-$ OPCs, which still harbor cilia (Figure S2A), which reflects the propensity for OPCs to tile and divide to replace missing neighboring OPCs.[8] Because non-recombined, ciliated $EYFP^-$ OPCs compensate for diminished $EYFP^+$ OPCs, we focus on the $EYFP^+$ cells in Ift88 cKO and controls.

To determine the cause of the reduction in density of $EYFP^+$ Ift88 cKO oligodendroglia, we administered the thymidine analog 5-ethynyl-2′-deoxyurdine (EdU) at P7 and P8 to label dividing cells and analyzed cortices at P11 (Figure 2D). We detected a significant reduction in the fraction of EdU^+EYFP^+ cells (50%) (Figure 2E) in Ift88 cKO, showing that OPCs lacking cilia fail to expand. To rule out a contribution of defects in specification or migration to this phenotype, we quantified the densities of $EYFP^+$ and $Pdgfr\alpha^+$ cells in the P0 cortex, as the final wave of specified OPCs emerge to populate the cortex. At P0, there is no significant difference between the number of $EYFP^+$ cells in the cortex of Ift88 cKO mice compared with controls, indicating that specification and migration occur normally and that the observed reduction in OPCs at P7 is due to the failure of recombined OPCs to expand in the absence of their cilia (Figures S4A–S4C). Oligodendroglia in Ift88 cKO also displayed no significant difference in expression of the cell death markers cleaved caspase-3 or TUNEL (terminal deoxynucleotidyl transferase dUTP nick end labeling) (Figures S3A and S3B), indicating that the loss of OPC cilia does not affect OPC survival. Furthermore,

we found that, while loss of OPC cilia reduced the density of EYFP$^+$CC1$^+$ differentiating OLs as a function of the reduction in the broader EYFP population, this was not due to a decrease in the ability of OPCs lacking cilia to differentiate. When generated, EYFP$^+$ cells in Ift88 cKO mice differentiate in proportions comparable with controls (Figure S2C). Taken together, these results show that loss of OPC cilia decreases normal developmental OPC proliferation.

Primary cilia are required for OPC proliferation in remyelination

Remyelination following white matter injury (WMI) is highly susceptible to failure in diseases such as MS and newborn hypoxic brain injury, but regulatory factors relevant in human myelin regeneration are unclear. Successful remyelination requires the recruitment of OPCs into areas of demyelination and their significant intralesional proliferation. To assess the function of primary cilia in OPC proliferation following WMI, we made use of tamoxifen-inducible platelet-derived growth factor α (Pdgfrα)-CreERT: ift88$^{fl/fl}$; RosaEYFP mice (referred to as Ift88 icKO (inducible conditional knockout) hereafter) to avoid any developmental defects from loss of OPC cilia. Littermates expressing Pdgfrα-CreERT and one WT Ift88 allele were used as controls. We induced recombination in these mice by administering tamoxifen at 4 weeks of age and verified that our tamoxifen injection paradigm resulted in recombination in OPCs in the adult mouse spinal cord using EYFP (Figures 2F and 2G; Figures S1E–S1G). Focal demyelination was produced in the mouse spinal cord in 10-week-old mutants and controls, and the lesion was subsequently assessed at 5 dpl, when peak OPC recruitment occurs in this WMI model. Conditional removal of Ift88 from EYFP$^+$ cells in remyelination resulted in a marked 75% reduction in the proportion of ciliated EYFP$^+$ oligodendroglia (EYFP$^+$Arl13b$^+$) (Figure 2H). Loss of OPC cilia also resulted in a significant 50% reduction in the density of EYFP$^+$ oligodendroglia populating the lesion (Figure 2I) in Ift88 cKO versus controls. However, as in development, the total number of Pdgfrα$^+$ cells within Ift88 icKO lesions remained unchanged, which we attribute to incomplete recombination in adult OPCs and a compensatory increase in proliferation of EYFP$^-$ OPCs, which still have cilia (Figure S2B). Our analyses therefore focused on the EYFP$^+$ population of cells in lesions.

To determine whether OPC cilia are required for the local proliferation of OPCs in WMI, we induced lysolecithin lesions and then injected EdU intraperitoneally (i.p.) at 3 dpl for subsequent assessment at 5 dpl in Ift88 icKO and controls. Removal of OPC cilia reduced the number of proliferating OPCs in lesions by 50% (EYF-P$^+$EdU$^+$: 31.38% + 1.69% in controls vs. 15.50% + 3.14% in Ift88 cKO) (Figure 2J). We observed no significant difference in OPCs expressing cleaved caspase 3 or TUNEL, indicating that loss of OPC cilia did not affect OPC survival signaling during lesion repair (Figures S3C and S3D). These results indicate that primary cilia are required for the OPC response to injury and function to promote OPC expansion within WM lesions.

Hh activity is unaffected by the loss of OPC cilia

Vertebrate primary cilia activate GLI transcription factors and generate GLI transcriptional repressors to regulate Hh signaling.[16,18,20,40] While there is strong evidence for the role of Hh signaling in OPC specification, there remain conflicting reports of the role of this

signaling pathway in oligodendroglial proliferation, differentiation, and involvement in injury repair. To assess whether primary cilia control Hh signaling in OPCs, we examined the expression of two Hh target genes, *Gli1* and *Ptch1*. In culture, there is a significant reduction in the proportion of ciliated OPCs isolated from P7 Ift88 cKO mice compared with controls (5.998% compared with 44.54%, p = 0.0004) (Figures S5A and S5B). qRT-PCR analysis of these isolated OPCs revealed no significant difference in *Gli1* or *Ptch1* expression in OPCs lacking cilia (Figure 3A). Because of the sustained expression of Hh target genes in Ift88 cKO, we sought to determine whether OPCs that have lost cilia are responsive to Hh signals. We treated OPCs isolated from P7 control and Ift88 cKO mice with 0, 10, or 50 nM Smo agonist (SAG) in cell medium. This was followed by treatment with EdU to label proliferating cells. Consistent with the observations from our *in vivo* studies, isolated Ift88 cKO OPCs exhibited a decrease in proliferation compared with controls with 0 nM SAG (Figures 3B and 3C). Interestingly, treatment with 10 or 50 nM SAG resulted in similar increases in proliferation in control and Ift88 cKO OPCs (Figures 3B and 3C). We assessed *Gli1* and *Ptch1* expression in OPCs after SAG treatment via qRT-PCR and established that *Gli1* and *Ptch1* expression increased similarly in control and Ift88 cKO OPCs in the presence of 10 and 50 nM SAG (Figure 3D). Together, these results show that Hh signaling and the ability to respond to Hh signals are unaltered in Ift88 cKO OPCs. It is possible that this unaltered responsiveness to Hh signals in OPCs lacking primary cilia is due to extraciliary Smo localization and activation. These data also point to a non-Hh mechanism of signal transduction in OPC cilia regulating proliferation.

The primary cilium controls OPC proliferation via regulation of CREB activity

To establish the signaling pathways affected in OPCs after removal of cilia, we used RNA sequencing (RNA-seq) to transcriptionally profile oligodendroglia isolated from the cortices of P11 Ift88 cKO mice and controls by fluorescence-activated cell sorting (FACS) (via endogenous EYFP expression). After verifying the reduction in Ift88 expression (p = 0.0287), we identified 443 significantly upregulated and 566 significantly downregulated ($p < 0.05$) genes in Ift88 cKO OPCs compared with control OPCs. Our RNA-seq data confirmed that loss of OPC cilia did not alter the expression of the common Hh targets *Gli1*, *Gli2*, *Gli3*, and *Smo* (Figure 4B). We compared our generated list of downregulated genes with existing ChIP-X datasets using Enrichr (https://maayanlab.cloud/Enrichr/enrich#). We noticed a significant overlap in genes associated with the CREB1 binding site (adjusted p = 6.8E−06) between our downregulated genes and transcription factors present in ENCODE and ChEA (chromatin immunoprecipitation [ChIP] enrichment analysis) (Figure 4A). Analysis of the significantly downregulated CREB1-associated genes from our dataset through a literature search revealed that *Hlf*, *Pde4a*, *Rnf40*, *Herc2*, *Eif3a*, *Jarid2*, *Cdkn1a*, *Becn1*, and *Id1* have been previously linked to cell cycle control and proliferation (Figure 4B).[40–47] qRT-PCR analysis of purified P7 Ift88 cKO and control OPCs confirmed that loss of OPC cilia decreases the expression of these genes (Figure 4C).

We explored the possibility that loss of OPC cilia affects CREB activity in OPCs. The initiation of CREB-dependent transcription requires CREB activation through phosphorylation by protein kinases.[48] OPCs isolated from P7 Ift88 cKO exhibited reduced expression of phosphorylated CREB (pCREB) (Ser133) compared with controls, suggesting

that removal of OPC cilia inhibits CREB activation (Figure 4D). To determine whether OPC proliferation requires CREB activation and subsequent CREB-mediated gene transcription, we used 666–15, a cell-permeable naphthol derivative and selective inhibitor of CREB-mediated gene transcription.[49] OPCs isolated from P7 WT rats displayed a significant reduction in proliferation when treated with 50 nM 666–15 compared with control DMSO (Figure 4E). 666–15 reduced pCREB (Ser133) expression in OPCs (Figures 4G and 4H) and expression of several of the differentially expressed CREB-associated genes identified from our RNA-seq analysis: *Rnf40*, *Herc2*, *Eif3a*, and *Jarid2* (Figure 4I), as analyzed via qRT-PCR. We hypothesized that, if CREB-mediated gene transcription regulates OPC proliferation, then selected CREB1-associated genes from our transcriptional analysis of Ift88 cKO OPCs would also be required for OPC proliferation. We generated shRNAs to silence the expression of these genes in P7 WT rat OPCs *in vitro*. Of these, knockdown of *Eif3a* and *Jarid2* significantly reduced OPC proliferation (Figure S6). Silencing *Cdkn1a* increased OPC proliferation (Figure S6), as expected, because *Cdkn1a* suppresses proliferation by inhibiting cell cycle progression.[46]

CREB1 is a downstream effector of cAMP, a secondary messenger involved in signaling cascades triggered by GPCRs. As a growing number of GPCRs are identified to be specifically targeted to mammalian cilia, the downregulation of genes associated with CREB1 binding in Ift88 cKO may indicate that loss of OPC cilia results in defective GPCR and cAMP signaling in OPCs. To determine whether the reduction of CREB activation observed in OPCs upon loss of cilia is due to attenuated cAMP production, we assessed cAMP levels in OPCs *in vitro* using a cAMP-Glo assay. Purified Ift88 cKO OPCs displayed a reduction in intracellular cAMP levels (Figure 4J). Overall, our data show that, in the absence of cilia, OPCs fail to proliferate because of attenuated cAMP levels and, consequently, decreased CREB-mediated transcription of genes linked to proliferation (e.g., *Jarid2* and *Eif3a*). Because cAMP notably lies downstream of GPCRs, this study points to a GPCR/cAMP/CREB signaling axis that is initiated at OPC primary cilia to promote OPC proliferation. A GPCR activated at the primary cilium could result in changes in cytoplasmic and ciliary cAMP levels (not distinguished in this study) that, in turn, impact CREB phosphorylation in the nucleus. pCREB then binds CRE to activate transcription factors modulating OPC proliferation (Figure 4J).

DISCUSSION

After insult to white matter, remyelination involves the enhanced migration, proliferation, and differentiation of OPCs in areas of injured and recovering tissue. The regeneration of myelin therefore depends on OPC activation and proliferation, but OPCs often remain depleted in chronically demyelinated lesions.[3,4] While the environmental and intrinsic systems regulating OPC proliferation have been studied extensively in development, these studies are sparse in the context of injury. Processes regulating developmental myelination are often recapitulated during remyelination, and factors controlling OPC proliferation during development can promote myelin regeneration after injury.[2] For instance, PDGF, fibroblast growth factor (FGF), and epidermal growth factor (EGF) are factors that have been shown to promote proliferation during development and in response to different models of WMI through their obligate receptors (Pdgfrα, FGFRs, and EGFRs, respectively).[50–53] In

this study, we find that remyelination requires OPC cilia and ciliary signaling because loss of cilia significantly reduces OPC proliferation in white matter lesions.

Primary cilia most commonly transduce Hh signals. In cultured rat OPCs, ciliobrevin, an AAA+ ATPase inhibitor that also causes cilium disassembly, destabilizes OPCs, while co-treatment with ciliobrevin and Shh preserves OPC morphology and ciliary assembly.[28] However, whether OPC cilia are required for Hh signal transduction has not been studied previously. In addition to the critical role of Hh in embryonic OPC specification,[32,54] several studies show that overexpression of Shh in the adult mouse corpus callosum under homeostatic conditions and after focal demyelination promotes Hh gene expression, OPC proliferation, and tissue preservation,[33,34] indicating that OPCs are responsive to Hh signals in different contexts. Surprisingly, our results show that cilia are not required for Hh signal transduction in OPCs. How are OPCs transducing Hh signals without the requisite ciliary accumulation of Smo? One possible explanation is that Hh pathway activation can occur in the absence of ciliary Smo accumulation. In the absence of OPC cilia, Hh ligand could be engaging extraciliary Smo activity to regulate Gli and promote Hh target gene expression.[55] We conclude that loss of cilia in OPCs produces proliferation deficits with intact canonical Hh signaling, pointing toward Hh-independent ciliary control of OPC proliferation. Our results do not address how Smo accumulates in the absence of cilia or whether Smo accumulates in OPC cilia when they are present. The conclusion we draw is that Hh signaling in OPCs does not require primary cilia and is not the mechanism underlying the proliferation deficit observed in Ift88 cKO mice.

This study reveals that loss of OPC cilia results in the downregulation of genes associated with CREB binding sites. CREB phosphorylation can occur in response to mitogens, and the function of CREB activation has been linked to proliferation in many cell types.[56,57] In the OL lineage, OPC proliferation follows the rapid stimulation of CREB phosphorylation upon exposure to neurotrophin (NT-3).[58] Our data are consistent with previous studies showing that CREB-mediated transcriptional changes can promote the proliferation and population maintenance of OPCs.[59] Still, CREB can be activated by a wide variety of stimuli but evoke extremely specific responses depending on the selective initiation of downstream gene transcription. The CREB response to signaling initiated at the cilium likely involves the transcription of a specific subset of factors that regulate proliferation and differ from gene transcription initiated from extraciliary signals. We identify *Eif3a* and *Jarid2* as genes downstream of ciliary CREB activation in OPCs, but their roles in OL biology are not defined. Studies in several cell types show that knockdown or mutations in *Eif3a* or *Jarid2* result in decreased proliferation,[44,45] providing a precedent for their role in promoting OPC proliferation.

To fully define the ciliary contribution to OPC proliferation would require the identification of cilium-localized upstream regulators of CREB activation. CREB lies downstream of kinases that are activated as a part of the cAMP signaling cascade. Because cAMP is the secondary effector for GPCR signal transduction, and GPCRs are enriched in primary cilia, a ciliary GPCR may be mediating OPC proliferation. Indeed, several GPCRs control OL development. GPR37, enriched in promyelinating and mature OLs but not OPCs, inhibits precocious myelination by inhibiting the cAMP/EPAC activation of ERK1/2.[60]

Gpr17 also inhibits myelination but via upregulation of the myelination inhibitors ID2/4.[36] GPR56, an adhesion GPCR, maintains OPC proliferation and inhibits differentiation in a RhoA-dependent manner.[37,38] Because Gpr17 and Gpr56 are expressed in OPCs, it would be interesting to determine whether they are enriched in OPC primary cilia. Multiple functional GPCRs could localize to OPC cilia. Instead of a straightforward model where one ciliary GPCR acts independently to affect changes in OPC biology, the intracellular changes observed upon removal of cilia in OPCs could be due to loss of a well-choreographed cross-talk between multiple ciliary GPCRs that fine-tune cAMP levels either in the cytoplasm or ciliary axoneme through enlisting a balance of stimulatory and inhibitory G-protein subunits. This adds yet another way in which signaling specificity can be achieved by OPCs.

Based on our findings, we propose a model where GPCR(s) enriched at the ciliary membrane of OPCs are activated by a cue that instructs OPC proliferation. This leads to downstream increases in total cAMP levels that instruct kinase(s) to phosphorylate CREB (Ser133) in the nucleus, which then binds to CRE (cAMP response element). This specific cascade, beginning from the cilium, ultimately activates the transcription of a distinct set of genes, including *Eif3a* and *Jarid2*, that mediate OPC proliferation. Therefore, we observe a decrease in OPC proliferation in Ift88 cKO mice because loss of Ift88 results in the disruption of this cascade of events. Without the cilium, a decrease in cAMP levels and concomitant loss of pCREB expression result in failure to initiate the transcription of genes regulating OPC proliferation. Some previous studies have suggested possible extraciliary functions for Ift88,[61–63] which could conceivably contribute to OPC proliferation control. Confirming that OPC proliferation requires OPC primary cilia will depend on an orthogonal method of cilium removal, such as loss of Tctn2 or Ofd1.[64]

While our study identifies a mechanism whereby signal transduction via OPC cilia activates CREB-mediated transcription to promote OPC proliferation, the true scope of the functional importance of OPC cilia remains unclear. The ciliary membrane is physically contiguous with the plasma membrane but molecularly distinct because of a transition zone at the base of the cilium that regulates protein trafficking in and out of the organelle.[65] With advancements in proximity-labeling technologies, it is now possible to consistently isolate and analyze proteins selectively localized to primary cilia.[26,66] Studies show that the composition of cilia can be dynamic[26,67] and clearly differs between cell types. For example, adenylate cyclase 3 is present in neuronal cilia but has been shown to fail to be detected in IMCD3 kidney cells.[66] The ciliary transition zone displays compositional differences between cell types.[68] Ciliary GPCRs also display regional specificity, as exemplified by differences in neuronal ciliary expression of somatostatin receptor 3,[23] the serotonin receptor 5-HT_6,[69] and melanocortin 4 receptor.[70] The compositional diversity of cilia across cell types highlights the potential for unique, cell-type-specific, proteomes. Identification of signaling proteins specific to OPC cilia and the downstream signaling cascades may provide fascinating insights into how specialized signaling occurs in OPCs. Future unbiased and comprehensive identification of proteins that survey OPC cilia through proteomics profiling[26,66] will reveal a list of signaling molecules that may be required for proper OPC function as well as ciliary GPCRs that may be the upstream effectors of cAMP and CREB activity in OPCs. It will also identify drug targets to promote OPC proliferation in white matter diseases.

Limitations of the study

Our study indicates that CREB-mediated gene transcription is significantly reduced in Ift88 cKO OPCs. The role of primary cilia in regulating OPC proliferation through mediating CREB activity is further supported by the observed reduction in OPC proliferation *in vitro* following pharmacological inhibition of CREB using 666–15. These results might suggest that potentiating CREB or cAMP signaling in Ift88 cKO OPCs would promote proliferation and rescue the observed phenotype. However, CREB does not simply initiate the transcription of all CRE-driven target genes upon its activation. CREB-mediated gene transcription is highly specific depending on upstream stimuli that instruct genes to be activated to generate a desired effect. Different stimuli are thus capable of dictating the transcription of distinct sets of CREB target genes.[71–73] Pharmacological potentiation of CREB activity using dBcAMP (a cell permeable synthetic analog of cAMP that mimics cAMP activity) or rolipram (a selective Pde4a inhibitor) would activate CREB in a non-specific manner. We currently do not have the tools readily available to reproduce the exact conditions that initiate the transcription of the specific set of CREB target genes that seem to mediate OPC proliferation. Rescuing the proliferation phenotype of Ift88 cKO OPCs by activating cAMP signaling and CREB-mediated transcription will require identifying the specific upstream pathway and ciliary receptor.

STAR★METHODS

RESOURCE AVAILABILITY

Lead contact—Further information and requests for resources and reagents should be directed to and will be fulfilled by the Lead Contact, Stephen Fancy (stephen.fancy@ucsf.edu).

Materials availability—All unique/stable reagents generated in this study are available from the lead contact without restriction.

Data and code availability

- RNA sequencing data were deposited in NCBI's Gene Expression Omnibus (GEO) and are publicly available under accession number GEO: GSE243997.
- This paper does not report original code.
- Additional information is available from the lead contact upon reasonable request.

EXPERIMENTAL MODEL AND SUBJECT DETAILS

Mice—All mice were handled according to guidelines set by the University of California, San Francisco and housed within a barrier facility on a 12-h light/dark cycle. Mice were housed with up to four other same-sex cage mates in standard rodent cages and provided food and water *ad libitum*. Both male and female mice were used for all experiments. All animal protocols and procedures were approved by UCSF's IACUC.

Pdgfra-Cre: These mice have been described previously[78] (JAX Stock No. 013148). These mice were crossed with Ift88 floxed and RosaEYFP mice to knockout Ift88 during development, and for purification of Ift88 knockout OPCs for *in vitro* studies. Ages studied were E13.5, P0, P7, P10, P11, and P60.

Pdgfra-CreERT: These mice have been described previously[79] (JAX Stock No. 018280). These mice were crossed with Ift88 floxed and RosaEYFP mice. Mice were given 2 mg tamoxifen (T-5648, Sigma) dissolved in 90% corn oil/10% ethanol intraperitoneally to induce recombination. Mice were studied at 10 weeks of age.

Ift88 floxed and RosaEYFP: These mice have been described previously and were generously provided by Dr. Jeremy Reiter[80,81] (University of California, San Francisco; Ift88 flox previously available from JAX Stock No. 022409; RosaEYFP available from JAX Stock No. 006148). Ift88 flox mice were crossed with Pdgfra-Cre mice to generate constitutive Ift88 knockout in OPCs (studied at E13.5, P0, P7, P10, P11, and P60) or Pdgfra-CreERT to generate tamoxifen-inducible, conditional Ift88 knockout in OPCs (studied at 10 weeks of age). These mice were also crossed with RosaEYFP mice to report recombination. Pdgfra-Cre: $Ift88^{fl/wt}$; RosaEYFP or Pdgfra-CreERT: $Ift88^{fl/wt}$; RosaEYFP were crossed to $Ift88^{fl/fl}$; RosaEYFP mice to generate experimental offspring and control littermates.

Oligodendrocyte precursor cell (OPC) cultures—Primary rat or mouse OPCs were isolated from the cortical hemispheres of postnatal day 7 rat or mouse cortices (Pdgfra-Cre: $Ift88^{fl/fl}$ and littermate controls) as previously described.[82] Briefly, rodent cortices were minced and dissociated in papain in 37°C with periodic shaking (Worthington) for 75 min (rat) or 60 min (mouse). After trituration, the suspension was immersed in 0.2% BSA at room temperature and underwent two sequential 30 min incubations in negative selection plates (Ran-2 and Gal-C) and one 45 min incubation for positive selection of OPCs (O4). Selection plates were prepared by incubating dishes with goat IgG and IgM secondary antibodies (Jackson ImmunoResearch) in 50 mM Tris-HCl overnight at room temperature. Antibodies Ran-2, Gal-C, or O4 were added after washing with DPBS (Invitrogen). Dissociation of OPCs from positive selection dish was performed using 0.05% Trypsin-EDTA (Invitrogen) and purified OPCs were seeded onto $12mm^2$ coverslips coated with poly-L-lysine (Sigma-Aldrich) at a density of 15,000 cells per coverslip. OPCs were maintained in DMEM (Invitrogen) supplemented with B27 (Invitrogen), N2 (Invitrogen), *N-acetylcysteine* (Sigma-Aldrich), forskolin (Sigma-Aldrich), penicillin-streptomycin (Invitrogen), and PDGF-AA (Peprotech) overnight at 37°C, 5% CO_2. For experiments involving SAG, purified P7 mouse Ift88 cKO and control OPCs were cultured in media containing SAG for 24 h. OPCs were then incubated in 10 μM EdU for 2 h to label proliferating cells. For experiments involving 666–15, purified P7 rat OPCs 666–15 was added to culture media for 8 h. OPCs were then incubated in 10 μM EdU for 2 h to label proliferating cells.

Lysolecithin lesion—The method has been described previously.[83] Focal demyelinated lesions were produced in the white matter of the spinal cord dorsal funiculus in 10-week-old Pdgfra-CreERT: $Ift88^{fl/fl}$; RosaEYFP and Pdgfra-CreERT: $Ift88^{fl/wt}$; RosaEYFP control

mice after tamoxifen treatment. We used inhalational isoflurane and oxygen supplemented with subcutaneously injected 0.05 mg/kg buprenorphine to induce and maintain anesthesia. The tissue was cleared surrounding the spinal vertebrae at T12/T13, and the underlying spinal cord pierced with a dental needle lateral to the midline. A Hamilton needle positioned at a 45° angle was then used to slowly inject 0.5 μL of 1% lysolecithin through the pierced dura into the white matter of the dorsal funiculus.

Human HIE tissue—All human tissue was collected with informed consent and following guidelines established by the Committee on Human Research at the University of California, San Francisco (H11170–19113-07), as previously described. Immediately upon collection, brains were immersed in 4% paraformaldehyde in PBS for 3 d. On day 3, the brain was cut coronally at the level of mammillary body and re-immersed in fresh 4% paraformaldehyde in PBS for an additional 3 d. Tissue samples were equilibrated in 30% sucrose in PBS for at least 2 d post-fixation then placed in molds and embedded in optimal cutting temperature medium for 30 min at room temperatures. Samples were then frozen in dry ice-chilled ethanol. Brain dissection and evaluation was performed by the neuropathology staff at UCSF. HIE diagnosis requires clinical and pathological correlation; no widely accepted diagnostic criteria are present for the pathological diagnosis of HIE.

METHOD DETAILS

Tamoxifen and EdU administration—Tamoxifen (T-5648, Sigma) was diluted in 90% corn oil/10% ethanol and administered intraperitoneally in Ift88 icKO mice and littermate controls starting at 4 weeks of age. 2 mg of tamoxifen was given to each mouse for 5 consecutive days, followed by a week of rest. The tamoxifen injection was repeated for a total of 15 tamoxifen injections per mouse. For animal EdU labeling experiments, EdU was diluted in a 4 mg/mL stock solution in sterile 1X PBS and injected intraperitoneally at a concentration of 40 mg/kg. For developmental studies, Ift88 cKO and control mice were injected at P7 and at P8. For remyelination studies, Ift88 icKO and control mice were injected once at 3 dpl.

Immunohistochemistry—Mice were perfused with PBS followed by 4% (w/v) paraformaldehyde (PFA) in PBS. Brains and spinal cords were dissected and post-fixed in 4% PFA for 6 h at 4°C. After post-fixation, tissue was cryoprotected using 30% (w/v) sucrose in PBS. Tissue was sectioned at 15 μm using a cryostat (Leica CM1950). Slides with sections were stored at −80°C until use. For immunohistochemical analysis, slides were thawed at room temperature, washed 3 times with PBS and blocked in PBS containing 10% normal goat serum and 0.1% Triton X-100 for 1 h at room temperature. Primary antibodies were diluted in 10% goat serum in PBS and incubated overnight at 4°C. Slides were then incubated in goat Alexa Fluor-conjugated secondary antibodies diluted in 10% goat serum in PBS and DAPI for 1 h at room temperature. The primary antibodies used were: rabbit polyclonal anti-Arl13b (Proteintech, 17711–1-AP, 1:1000), mouse anti-Arl13b (NIH Neuromab facility, 73–287, 1:500), rabbit anti-Pdgfra (gift from W. Stallcup), rat monoclonal anti-Pdgfra (BD Biosciences, 558774, 1:200), mouse monoclonal anti-CC1 (Millpore, OP80, 1:500), rat monoclonal anti-MBP (Bio-Rad, MCA409S, 1:1000), chicken polyclonal anti-GFP (Aves Labs, GFP-1020, 1:1000), rabbit monoclonal anti-GFP (Thermo

Fisher, G10362, 1:1000), rabbit polyclonal anti-Olig2 (Millipore, AB9610, 1:1000), mouse monoclonal anti-Olig2 (Millipore, MABN50), rabbit polyclonal anti-cleaved caspase-3 (Cell Signaling Technology, 9661, 1:500), rabbit polyclonal anti-IFT88 (Proteintech, 13967–1-AP, 1:500). EdU was detected in proliferating cells using the Click-IT EdU Cell Proliferation Kit for Imaging (Invitrogen C10340) according to manufacturer's instructions. Tissue sections were incubated in the reaction mix for 30 min at room temperature following secondary antibody incubation. Images were obtained on a Zeiss Axio Imager Z1 microscope. TUNEL assay was performed using the *In Situ* Cell Death Detection Kit (Roche, 12156792910).

OPC cultures were fixed in 4% (w/v) paraformaldehyde (PFA) in DPBS for 15 min and dehydrated. Cultures were blocked and permeabilized in 10% goat serum in DPBS containing 0.1% (v/v) Triton X-100 for 1 h at room temperature. Primary antibodies were diluted in 10% goat serum and incubated overnight at 4°C. Secondary antibodies were diluted in 10% goat serum with DAPI and incubated for 1 h at room temperature. The following primary antibodies were used: rabbit polyclonal anti-Arl13b (Proteintech, 17711–1-AP, 1:1000), rat monoclonal anti-Pdgfra (BD Biosciences, 558774, 1:200), rabbit anti-Pdgfra (gift from W. Stallcup), rat monoclonal anti-MBP (Bio-Rad, MCA409S, 1:1000), and chicken polyclonal anti-GFP (Aves Labs, GFP-1020, 1:1000). Alexa Fluor-conjugated secondary antibodies (rat, rabbit, 1:1000) were used to detect fluorescence. The incorporation of EdU by proliferating cells was detected via the Click-iT EdU Cell Proliferation Kit (Invitrogen C10340) after incubation in primary and secondary antibodies. Images were obtained on a Zeiss Axio Imager Z1 microscope. Cells were quantified from randomly selected fields of view per coverslip under 10x magnification.

Sample preparation for immunogold labeling—Mice were anesthetized with avertin. Fixation was performed by intracardiac perfusion with 0.9% saline solution/0.01% heparin for 5 min, followed by 15 min with 3%PFA/1% glutaraldehyde in PBS. The brain was extracted and post-fixed in the same solution overnight. Finally, brains were washed 3 times for 10 min in 1X PBS and stored in PBS/0.05% sodium azide until processing.

Brains were sectioned at 50 μm using a Leica VT1000S vibratome (Leica Biosystems, Wetzlar, Germany) and sections were stored in 0.1M phosphate buffer (PB)/0.05% sodium azide.

Immunogold labeling—Tissue sections were cryoprotected in a solution containing 25% saccharose in 0.1M PB/0.05% azide for 30 min. Immediately after cryoprotection, sections were permeabilized by immersion in −60°C 2-methylbutane and rapidly transferred to a room temperature saccharose solution. This step was repeated twice. Subsequently, tissue sections were left in 0.1M PB and then incubated in primary antibody blocking solution [0.3% BSAc (Aurion, Wageningen, The Netherlands), 0.05% sodium azide in 0.1 M PB] for 1 h. Next, the samples were incubated in primary antibody [1:200 chicken anti-GFP (Aveslab)] in primary antibody blocking solution for 72 h at 4°C. The samples were then rinsed in 0.1 M PB and incubated in secondary antibody blocking solution consisting of 0.5% BSAc (Aurion), 0.025% CWFS gelatin (Aurion), 0.05% sodium azide in 0.1 M PB for 1 h, followed by incubation in secondary antibody [1:50 goat anti-chicken IgG gold ultrasmall (Aurion)] diluted in the same secondary antibody blocking solution overnight

at 4°C. To enhance gold labeling, we performed silver enhancement (R-GENT SE-LM, Aurion) for 25 min in the dark, followed by gentle washing in 2% sodium acetate and incubation in gold toning solution (0.05% gold chloride in water) for 10 min. The samples were then washed twice with 0.3% sodium thiosulfate in water. Finally, we post-fixed with 2% glutaraldehyde (Electron Microscopy Sciences) in 0.1 M PB for 30 min. Samples were rinsed and kept in 0.1 M PB containing 0.05% sodium azide at 4°C until processing them for resin embedding.

Electron microscopy processing—For transmission electron microscopy, sections were embedded in epoxy resin. First, samples were post-fixed with 1% osmium tetroxide (Electron Microscopy Sciences), 7% glucose in 0.1 M PB for 30 min at room temperature, washed in deionized water, and partially dehydrated in 70% ethanol. Afterward, the samples were contrasted in 2% uranyl acetate (Electron Microscopy Sciences) in 70% ethanol for 2 h at 4°C. The samples were further dehydrated and embedded in Durcupan ACM epoxy resin at room temperature overnight, and then at 70°C for 72 h. Once the resin was polymerized, immunolabeled sections were selected and cut into serial semithin (1.5 mm) and then into serial ultrathin sections (60–80 nm) using an Ultracut UC7 ultramicrotome (Leica). We examined 20–25 serial ultrathin sections per cell. Ultrathin sections were placed on formvar-coated single-slot copper grids (Electron Microscopy Sciences) stained with lead citrate and examined at 80 kV on a FEI Tecnai G2 Spirit (FEI Company, Hillsboro, OR) transmission electron microscope equipped with a Morada CCD digital camera (Olympus, Tokyo, Japan).

RT-qPCR—RNA was extracted from OPC cultures using RNeasy Mini kit (Qiagen) following manufacturer's instructions. Purified RNA was reverse transcribed to cDNA using the iScript cDNA Synthesis Kit (Bio-Rad) following manufacturer's instructions. RT-qPCR was then performed in technical triplicates with the Power SYBR Green PCR Master Mix (Applied Biosystems) and QuantStudio 3 Real-Time PCR System (Thermo Fisher). Relative expression was calculated using the ΔΔCT method normalized to Gapdh expression. For RT-qPCR of CREB associated genes, Gli1 and Ptch1 in Ift88 cKO OPCs, data were normalized to OPCs isolated from littermate control mice. For RT-qPCR of CREB-associated genes after treatment with CREB inhibitor 666–15, data were normalized to OPCs treated with DMSO. (Primers in key resources table).

Flow cytometry/Fluorescence-activated cell sorting—Cells were isolated from P11 mouse cortices (control and Ift88 cKO). Briefly, mouse cortices were minced and dissociated in papain in 37°C with periodic shaking (Worthington) for 60 min. The suspension was filtered and pelleted at 1300 rpm for 5 min at 4°C. Pellets were resuspended in 22% Percoll (GE Healthcare) and centrifuged at 560g for 10 min at 4°C with no brake. After removal of myelin and debris, pelleted cells were resuspended in 2 mL of DMEM (Invitrogen) supplemented with B27 (Invitrogen), N2 (Invitrogen), *N-acetylcysteine* (Sigma-Aldrich), forskolin (Sigma-Aldrich), penicillin-streptomycin (Invitrogen), and PDGF-AA (Peprotech) and transferred to a glass tube for sorting. Cells were sorted based on EYFP fluorescence on a BD FACS Aria III and gated on forward/side scatter.

RNA-sequencing—For RNA-sequencing, a total of 3 control and 3 Ift88 cKO samples were used. For each sample, OPCs were isolated from the cortices of 4–6 mice and sorted on BD FACS Aria III flow cytometer via endogenous EYFP expression into RLT plus buffer (Qiagen). RNA was extracted and purified using an RNeasy Mini Kit (Qiagen). Libraries for RNA-seq were prepared using the QuantSeq 3′ mRNA-Seq Library Prep Kit FWD (Lexogen) following manufacturer's instructions and sequenced 50-bp single-end on the HiSeq 4000 (Illumina). This data has been deposited in NCBI's Gene Expression Omnibus and is accessible under accession GEO: GSE243997. FastQC (http://www.bioinformatics.babraham.ac.uk/projects/fastqc) was used to assess quality of fastq files. These were aligned to the mouse reference genome GRCm39 using the STAR aligner.[76] Differential expression analysis was performed using DESeq2.[77] Pairwise comparisons were performed between control and Ift88 knockout OPCs. Genes were selected by a significance threshold of $p < 0.05$, log2FC > 1 or log2FC < −1.

SDS-PAGE and western blotting—OPCs were purified from rat or mouse cortices. Cells were lysed in ice-cold RIPA buffer containing protease inhibitor, agitated for 30 min at 4°C, and sonicated 3 times for 10 s. The sample was centrifuged at 16000 x g for 20 min at 4°C and pellet discarded. Protein concentrations were determined using BCA protein assay kit (Thermo Fisher). Samples were run on 10% precast TGX gels (Bio-Rad) and transferred to PVDF membranes, blocked with 3% BSA in TBS-T for 1 h at room temperature, incubated with rabbit monoclonal anti-phosphorylated CREB antibody (Cell Signaling Technology, 9198, 1:1000) or rabbit polyclonal anti-β-actin antibody (Proteintech, 20536-1-AP, 1:1000) at 4°C overnight, followed by washes and secondary antibody (LICOR IRDye, 1:2000) at room temperature for 1 h. Images were acquired on a Li-Cor Odyssey scanner.

cAMP Measurements—To assess cAMP levels in Ift88 cKO OPCs and controls, we used the cAMP-Glo kit (Promega). OPCs were seeded into 12-well plates at a density of 50,000 cells per well in media containing PDGF-AA as described above. PDGF-AA was then removed from media for 4 h and incubated in cAMP-Glo Lysis Buffer and transferred to 96 well plates. cAMP-Glo assay was performed according to manufacturer's instructions, and plates were read using a microplate reader luminometer.

shRNA and lentiviral transduction—shRNAs were cloned in pSiCoR vectors (Addgene, 11579). For the generation of lentivirus containing shRNA vectors, lentivirus was produced in HEK293FT cells. HEK293FT cells were co-transfected with the appropriate lentiviral vector and packaging plasmids psPAX2 and pMD2.G at a 0.50:025:0.25 ratio using polyethylenimine (PEI) at a 1:3 DNA:PEI ratio. Cells were initially cultured in DMEM containing 10% FBS for 24 h, after which the media was changed to OPC culture media as described above. The viral supernatant was collected at 48 h post-transfection, filtered, and used for infection of OPCs with Polybrene reagent (EMD Millipore, 1:500).

QUANTIFICATIONS AND STATISTICAL ANALYSIS

Quantifications—All images were acquired on a Zeiss Axio Imager Z1 microscope. For quantifications in OPC cultures, cells were quantified from eight randomly selected fields

of view per coverslip under 10x magnification. Sample size (n) for cell culture experiments indicates number of independent experiments. For quantifications of cells in the mouse cortex, two fields were manually quantified per section in Fiji, using three averaged sections per mice. Sections were anatomically matched across mice. For density quantifications in dorsal funiculus spinal cord lesions, the number of $EYFP^+$ cells were divided by the area of the lesion per section. This value was averaged across three lesioned spinal cord sections per mice. Sample size (n) for animal experiments indicates number of mice used per experiment. Each individual data point represents average values per mouse. All image quantifications were conducted blinded.

Statistical analysis—Statistical analyses and graphing were performed using GraphPad Prism 9 software. We used unpaired t-tests to determine the statistical significance between two experimental groups (between genotypes or treatment conditions). For more than two samples, significance was determined via one-way ANOVA with Dunnett's post-hoc analysis or two-way ANOVA with Tukey's post-hoc analysis for two variables. For dot plots and bar graphs, data are presented as mean ± SEM. For box-and-whisker plots, the center represents the median while the box represents the interquartile range with whiskers indicating minimum and maximum values. A threshold of $p < 0.05$ was considered statistically significant. Statistical significance is denoted with the following symbols: ns indicates not significant, *$p < 0.05$, **$p < 0.01$, ***$p < 0.001$, and ****$p < 0.0001$.

Supplementary Material

Refer to Web version on PubMed Central for supplementary material.

ACKNOWLEDGMENTS

J.F.R. is supported by grants from the NIH (R01AR054396 and R01HD089918). S.P.J.F. is supported by grants from the NIH/NINDS (R01NS128021, P01NS083513, and R21NS133891), Race to Erase MS, and Alex's Lemonade Stand Foundation. S.P.J.F. is a Harry Weaver Neuroscience Scholar of the National Multiple Sclerosis Society.

INCLUSION AND DIVERSITY

We support inclusive, diverse, and equitable conduct of research.

REFERENCES

1. Fancy SPJ, Chan JR, Baranzini SE, Franklin RJM, and Rowitch DH (2011). Myelin regeneration: a recapitulation of development? Annu. Rev. Neurosci. 34, 21–43. 10.1146/annurev-neuro-061010-113629. [PubMed: 21692657]
2. Gallo V, and Deneen B (2014). Glial development: the crossroads of regeneration and repair in the CNS. Neuron 83, 283–308. 10.1016/j.neuron.2014.06.010. [PubMed: 25033178]
3. Lucchinetti C, Brück W, Parisi J, Scheithauer B, Rodriguez M, and Lassmann H (1999). A quantitative analysis of oligodendrocytes in multiple sclerosis lesions. A study of 113 cases. Brain 122, 2279–2295. 10.1093/brain/122.12.2279. [PubMed: 10581222]
4. Boyd A, Zhang H, and Williams A (2013). Insufficient OPC migration into demyelinated lesions is a cause of poor remyelination in MS and mouse models. Acta Neuropathol. 125, 841–859. 10.1007/s00401-013-1112-y. [PubMed: 23595275]
5. Bergles DE, and Richardson WD (2015). Oligodendrocyte Development and Plasticity. Cold Spring Harbor Perspect. Biol. 8, a020453. 10.1101/cshperspect.a020453.

6. Bradl M, and Lassmann H (2010). Oligodendrocytes: biology and pathology. Acta Neuropathol. 119, 37–53. 10.1007/s00401-009-0601-5. [PubMed: 19847447]
7. Elbaz B, and Popko B (2019). Molecular Control of Oligodendrocyte Development. Trends Neurosci. 42, 263–277. 10.1016/j.tins.2019.01.002. [PubMed: 30770136]
8. Hughes EG, Kang SH, Fukaya M, and Bergles DE (2013). Oligodendrocyte progenitors balance growth with self-repulsion to achieve homeostasis in the adult brain. Nat. Neurosci. 16, 668–676. 10.1038/nn.3390. [PubMed: 23624515]
9. Singla V, and Reiter JF (2006). The primary cilium as the cell's antenna: signaling at a sensory organelle. Science 313, 629–633. 10.1126/science.1124534. [PubMed: 16888132]
10. Pedersen LB, and Rosenbaum JL (2008). Intraflagellar transport (IFT) role in ciliary assembly, resorption and signalling. Curr. Top. Dev. Biol. 85, 23–61. 10.1016/S0070-2153(08)00802-8. [PubMed: 19147001]
11. Follit JA, Xu F, Keady BT, and Pazour GJ (2009). Characterization of mouse IFT complex B. Cell Motil Cytoskeleton 66, 457–468. 10.1002/cm.20346. [PubMed: 19253336]
12. Rosenbaum JL, and Witman GB (2002). Intraflagellar transport. Nat. Rev. Mol. Cell Biol. 3, 813–825. 10.1038/nrm952. [PubMed: 12415299]
13. Boehlke C, Kotsis F, Buchholz B, Powelske C, Eckardt KU, Walz G, Nitschke R, and Kuehn EW (2013). Kif3a guides microtubular dynamics, migration and lumen formation of MDCK cells. PLoS One 8, e62165. 10.1371/journal.pone.0062165. [PubMed: 23658710]
14. Corbit KC, Shyer AE, Dowdle WE, Gaulden J, Singla V, Chen MH, Chuang PT, and Reiter JF (2008). Kif3a constrains beta-catenin-dependent Wnt signalling through dual ciliary and non-ciliary mechanisms. Nat. Cell Biol. 10, 70–76. 10.1038/ncb1670. [PubMed: 18084282]
15. Kim M, Suh YA, Oh JH, Lee BR, Kim J, and Jang SJ (2016). KIF3A binds to β-arrestin for suppressing Wnt/β-catenin signalling independently of primary cilia in lung cancer. Sci. Rep. 6, 32770. 10.1038/srep32770. [PubMed: 27596264]
16. Corbit KC, Aanstad P, Singla V, Norman AR, Stainier DYR, and Reiter JF (2005). Vertebrate Smoothened functions at the primary cilium. Nature 437, 1018–1021. 10.1038/nature04117. [PubMed: 16136078]
17. Huangfu D, Liu A, Rakeman AS, Murcia NS, Niswander L, and Anderson KV (2003). Hedgehog signalling in the mouse requires intraflagellar transport proteins. Nature 426, 83–87. 10.1038/nature02061. [PubMed: 14603322]
18. Gigante ED, and Caspary T (2020). Signaling in the Primary Cilium through the Lens of the Hedgehog Pathway9 (Wiley Interdiscip Rev Dev Biol), p. e377. 10.1002/wdev.377.
19. Anvarian Z, Mykytyn K, Mukhopadhyay S, Pedersen LB, and Christensen ST (2019). Cellular signalling by primary cilia in development, organ function and disease. Nat. Rev. Nephrol. 15, 199–219. 10.1038/s41581-019-0116-9. [PubMed: 30733609]
20. Goetz SC, and Anderson KV (2010). The primary cilium: a signalling centre during vertebrate development. Nat. Rev. Genet. 11, 331–344. 10.1038/nrg2774. [PubMed: 20395968]
21. May SR, Ashique AM, Karlen M, Wang B, Shen Y, Zarbalis K, Reiter J, Ericson J, and Peterson AS (2005). Loss of the retrograde motor for IFT disrupts localization of Smo to cilia and prevents the expression of both activator and repressor functions of Gli. Dev. Biol. 287, 378–389. 10.1016/j.ydbio.2005.08.050. [PubMed: 16229832]
22. Mykytyn K, and Askwith C (2017). G-Protein-Coupled Receptor Signaling in Cilia. Cold Spring Harbor Perspect. Biol. 9, a028183. 10.1101/cshperspect.a028183.
23. Händel M, Schulz S, Stanarius A, Schreff M, Erdtmann-Vourliotis M, Schmidt H, Wolf G, and Höllt V (1999). Selective targeting of somatostatin receptor 3 to neuronal cilia. Neuroscience 89, 909–926. 10.1016/s0306-4522(98)00354-6. [PubMed: 10199624]
24. Einstein EB, Patterson CA, Hon BJ, Regan KA, Reddi J, Melnikoff DE, Mateer MJ, Schulz S, Johnson BN, and Tallent MK (2010). Somatostatin signaling in neuronal cilia is critical for object recognition memory. J. Neurosci. 30, 4306–4314. 10.1523/JNEUROSCI.5295-09.2010. [PubMed: 20335466]
25. Mukhopadhyay S, Wen X, Ratti N, Loktev A, Rangell L, Scales SJ, and Jackson PK (2013). The ciliary G-protein-coupled receptor Gpr161 negatively regulates the Sonic hedgehog pathway via cAMP signaling. Cell 152, 210–223. 10.1016/j.cell.2012.12.026. [PubMed: 23332756]

26. May EA, Kalocsay M, D'Auriac IG, Schuster PS, Gygi SP, Nachury MV, and Mick DU (2021). Time-resolved proteomics profiling of the ciliary Hedgehog response. J. Cell Biol. 220, e202007207. 10.1083/jcb.202007207. [PubMed: 33856408]
27. Truong ME, Bilekova S, Choksi SP, Li W, Bugaj LJ, Xu K, and Reiter JF (2021). Vertebrate cells differentially interpret ciliary and extraciliary cAMP. Cell 184, 2911–2926.e18. 10.1016/j.cell.2021.04.002. [PubMed: 33932338]
28. Falcón-Urrutia P, Carrasco CM, Lois P, Palma V, and Roth AD (2015). Shh Signaling through the Primary Cilium Modulates Rat Oligodendrocyte Differentiation. PLoS One 10, e0133567. 10.1371/journal.pone.0133567. [PubMed: 26218245]
29. Cullen CL, O'Rourke M, Beasley SJ, Auderset L, Zhen Y, Pepper RE, Gasperini R, and Young KM (2021). Kif3a deletion prevents primary cilia assembly on oligodendrocyte progenitor cells, reduces oligodendrogenesis and impairs fine motor function. Glia 69, 1184–1203. 10.1002/glia.23957. [PubMed: 33368703]
30. Delfino G, Bénardais K, Graff J, Samama B, Antal MC, Ghandour MS, and Boehm N (2022). Oligodendroglial primary cilium heterogeneity during development and demyelination/remyelination. Front. Cell. Neurosci. 16, 1049468. 10.3389/fncel.2022.1049468. [PubMed: 36505511]
31. Merchán P, Bribián A, Sánchez-Camacho C, Lezameta M, Bovolenta P, and de Castro F (2007). Sonic hedgehog promotes the migration and proliferation of optic nerve oligodendrocyte precursors. Mol. Cell. Neurosci. 36, 355–368. 10.1016/j.mcn.2007.07.012. [PubMed: 17826177]
32. Tekki-Kessaris N, Woodruff R, Hall AC, Gaffield W, Kimura S, Stiles CD, Rowitch DH, and Richardson WD (2001). Hedgehog-dependent oligodendrocyte lineage specification in the telencephalon. Development 128, 2545–2554. 10.1242/dev.128.13.2545. [PubMed: 11493571]
33. Ferent J, Zimmer C, Durbec P, Ruat M, and Traiffort E (2013). Sonic Hedgehog signaling is a positive oligodendrocyte regulator during demyelination. J. Neurosci. 33, 1759–1772. 10.1523/JNEURO-SCI.3334-12.2013. [PubMed: 23365216]
34. Loulier K, Ruat M, and Traiffort E (2006). Increase of proliferating oligodendroglial progenitors in the adult mouse brain upon Sonic hedgehog delivery in the lateral ventricle. J. Neurochem. 98, 530–542. 10.1111/j.1471-4159.2006.03896.x. [PubMed: 16805844]
35. Xu X, Yu Q, Fang M, Yi M, Yang A, Xie B, Yang J, Zhang Z, Dai Z, and Qiu M (2020). Stage-specific regulation of oligodendrocyte development by Hedgehog signaling in the spinal cord. Glia 68, 422–434. 10.1002/glia.23729. [PubMed: 31605511]
36. Chen Y, Wu H, Wang S, Koito H, Li J, Ye F, Hoang J, Escobar SS, Gow A, Arnett HA, et al. (2009). The oligodendrocyte-specific G protein-coupled receptor GPR17 is a cell-intrinsic timer of myelination. Nat. Neurosci. 12, 1398–1406. 10.1038/nn.2410. [PubMed: 19838178]
37. Ackerman SD, Garcia C, Piao X, Gutmann DH, and Monk KR (2015). The adhesion GPCR Gpr56 regulates oligodendrocyte development via interactions with Ga12/13 and RhoA. Nat. Commun. 6, 6122. 10.1038/ncomms7122. [PubMed: 25607772]
38. Giera S, Deng Y, Luo R, Ackerman SD, Mogha A, Monk KR, Ying Y, Jeong SJ, Makinodan M, Bialas AR, et al. (2015). The adhesion G protein-coupled receptor GPR56 is a cell-autonomous regulator of oligodendrocyte development. Nat. Commun. 6, 6121. 10.1038/ncomms7121. [PubMed: 25607655]
39. Seeley ES, and Nachury MV (2010). The perennial organelle: assembly and disassembly of the primary cilium. J. Cell Sci. 123, 511–518. 10.1242/jcs.061093. [PubMed: 20144999]
40. Komorowska K, Doyle A, Wahlestedt M, Subramaniam A, Debnath S, Chen J, Soneji S, Van Handel B, Mikkola HKA, Miharada K, et al. (2017). Hepatic Leukemia Factor Maintains Quiescence of Hematopoietic Stem Cells and Protects the Stem Cell Pool during Regeneration. Cell Rep. 21, 3514–3523. 10.1016/j.celrep.2017.11.084. [PubMed: 29262330]
41. Pullamsetti SS, Banat GA, Schmall A, Szibor M, Pomagruk D, Hänze J, Kolosionek E, Wilhelm J, Braun T, Grimminger F, et al. (2013). Phosphodiesterase-4 promotes proliferation and angiogenesis of lung cancer by crosstalk with HIF. Oncogene 32, 1121–1134. 10.1038/onc.2012.136. [PubMed: 22525277]

42. Xie W, Miehe M, Laufer S, and Johnsen SA (2020). The H2B ubiquitin-protein ligase RNF40 is required for somatic cell reprogramming. Cell Death Dis. 11, 287. 10.1038/s41419-020-2482-4. [PubMed: 32341358]
43. Cubillos-Rojas M, Schneider T, Hadjebi O, Pedrazza L, de Oliveira JR, Langa F, Guénet JL, Duran J, de Anta JM, Alcántara S, et al. (2016). The HERC2 ubiquitin ligase is essential for embryonic development and regulates motor coordination. Oncotarget 7, 56083–56106. 10.18632/oncotarget.11270. [PubMed: 27528230]
44. Fang C, Chen YX, Wu NY, Yin JY, Li XP, Huang HS, Zhang W, Zhou HH, and Liu ZQ (2017). MiR-488 inhibits proliferation and cisplatin sensibility in non-small-cell lung cancer (NSCLC) cells by activating the eIF3a-mediated NER signaling pathway. Sci. Rep. 7, 40384. 10.1038/srep40384. [PubMed: 28074905]
45. Cervantes S, Fontcuberta-PiSunyer M, Servitja JM, Fernandez-Ruiz R, García A, Sanchez L, Lee YS, Gomis R, and Gasa R (2017). Late-stage differentiation of embryonic pancreatic b-cells requires Jarid2. Sci. Rep. 7, 11643. 10.1038/s41598-017-11691-2. [PubMed: 28912479]
46. Miyatsuka T, Kosaka Y, Kim H, and German MS (2011). Neurogenin3 inhibits proliferation in endocrine progenitors by inducing Cdkn1a. Proc. Natl. Acad. Sci. USA 108, 185–190. 10.1073/pnas.1004842108. [PubMed: 21173230]
47. Ding BS, Nolan DJ, Butler JM, James D, Babazadeh AO, Rosenwaks Z, Mittal V, Kobayashi H, Shido K, Lyden D, et al. (2010). Inductive angiocrine signals from sinusoidal endothelium are required for liver regeneration. Nature 468, 310–315. 10.1038/nature09493. [PubMed: 21068842]
48. Shaywitz AJ, and Greenberg ME (1999). CREB: a stimulus-induced transcription factor activated by a diverse array of extracellular signals. Annu. Rev. Biochem. 68, 821–861. 10.1146/annurev.biochem.68.1.821. [PubMed: 10872467]
49. Xie F, Li BX, Kassenbrock A, Xue C, Wang X, Qian DZ, Sears RC, and Xiao X (2015). Identification of a Potent Inhibitor of CREB-Mediated Gene Transcription with Efficacious in Vivo Anticancer Activity. J. Med. Chem. 58, 5075–5087. 10.1021/acs.jmedchem.5b00468. [PubMed: 26023867]
50. Calver AR, Hall AC, Yu WP, Walsh FS, Heath JK, Betsholtz C, and Richardson WD (1998). Oligodendrocyte population dynamics and the role of PDGF in vivo. Neuron 20, 869–882. 10.1016/s0896-6273(00)80469-9. [PubMed: 9620692]
51. Redwine JM, and Armstrong RC (1998). In vivo proliferation of oligodendrocyte progenitors expressing PDGFalphaR during early remyelination. J. Neurobiol. 37, 413–428. [PubMed: 9828047]
52. Messersmith DJ, Murtie JC, Le TQ, Frost EE, and Armstrong RC (2000). Fibroblast growth factor 2 (FGF2) and FGF receptor expression in an experimental demyelinating disease with extensive remyelination. J. Neurosci. Res. 62, 241–256. 10.1002/1097-4547(20001015)62:2<241::AID-JNR9>3.0.CO;2-D. [PubMed: 11020217]
53. Scafidi J, Hammond TR, Scafidi S, Ritter J, Jablonska B, Roncal M, Szigeti-Buck K, Coman D, Huang Y, McCarter RJ, et al. (2014). Intranasal epidermal growth factor treatment rescues neonatal brain injury. Nature 506, 230–234. 10.1038/nature12880. [PubMed: 24390343]
54. Spassky N, Heydon K, Mangatal A, Jankovski A, Olivier C, Queraud-Lesaux F, Goujet-Zalc C, Thomas JL, and Zalc B (2001). Sonic hedgehog-dependent emergence of oligodendrocytes in the telencephalon: evidence for a source of oligodendrocytes in the olfactory bulb that is independent of Pdgfralpha signaling. Development 128, 4993–5004. 10.1242/dev.128.24.4993. [PubMed: 11748136]
55. Fan CW, Chen B, Franco I, Lu J, Shi H, Wei S, Wang C, Wu X, Tang W, Roth MG, et al. (2014). The Hedgehog pathway effector smoothened exhibits signaling competency in the absence of ciliary accumulation. Chem. Biol. 21, 1680–1689. 10.1016/j.chembiol.2014.10.013. [PubMed: 25484239]
56. Lee MM, Badache A, and DeVries GH (1999). Phosphorylation of CREB in axon-induced Schwann cell proliferation. J. Neurosci. Res. 55, 702–712. 10.1002/(SICI)1097-4547(19990315)55:6<702::AID-JNR5>3.0.CO;2-N. [PubMed: 10220111]
57. Long F, Schipani E, Asahara H, Kronenberg H, and Montminy M (2001). The CREB family of activators is required for endochondral bone development. Development 128, 541–550. 10.1242/dev.128.4.541. [PubMed: 11171337]

58. Johnson JR, Chu AK, and Sato-Bigbee C (2000). Possible role of CREB in the stimulation of oligodendrocyte precursor cell proliferation by neurotrophin-3. J. Neurochem. 74, 1409–1417. 10.1046/j.1471-4159.2000.0741409.x. [PubMed: 10737596]
59. Adams KL, Dahl KD, Gallo V, and Macklin WB (2021). Intrinsic and extrinsic regulators of oligodendrocyte progenitor proliferation and differentiation. Semin. Cell Dev. Biol. 116, 16–24. 10.1016/j.semcdb.2020.10.002. [PubMed: 34110985]
60. Yang HJ, Vainshtein A, Maik-Rachline G, and Peles E (2016). G protein-coupled receptor 37 is a negative regulator of oligodendrocyte differentiation and myelination. Nat. Commun. 7, 10884. 10.1038/ncomms10884. [PubMed: 26961174]
61. Boehlke C, Janusch H, Hamann C, Powelske C, Mergen M, Herbst H, Kotsis F, Nitschke R, and Kuehn EW (2015). A Cilia Independent Role of Ift88/Polaris during Cell Migration. PLoS One 10, e0140378. 10.1371/journal.pone.0140378. [PubMed: 26465598]
62. Robert A, Margall-Ducos G, Guidotti JE, Brégerie O, Celati C, Bréchot C, and Desdouets C (2007). The intraflagellar transport component IFT88/polaris is a centrosomal protein regulating G1-S transition in non-ciliated cells. J. Cell Sci. 120, 628–637. 10.1242/jcs.03366. [PubMed: 17264151]
63. Delaval B, Bright A, Lawson ND, and Doxsey S (2011). The cilia protein IFT88 is required for spindle orientation in mitosis. Nat. Cell Biol. 13, 461–468. 10.1038/ncb2202. [PubMed: 21441926]
64. Valente EM, Rosti RO, Gibbs E, and Gleeson JG (2014). Primary cilia in neurodevelopmental disorders. Nat. Rev. Neurol. 10, 27–36. 10.1038/nrneurol.2013.247. [PubMed: 24296655]
65. Gonçalves J, and Pelletier L (2017). The Ciliary Transition Zone: Finding the Pieces and Assembling the Gate. Mol. Cell. 40, 243–253. 10.14348/molcells.2017.0054.
66. Mick DU, Rodrigues RB, Leib RD, Adams CM, Chien AS, Gygi SP, and Nachury MV (2015). Proteomics of Primary Cilia by Proximity Labeling. Dev. Cell 35, 497–512. 10.1016/j.devcel.2015.10.015. [PubMed: 26585297]
67. Brewer KM, Engle SE, Bansal R, Brewer KK, Jasso KR, McIntyre JC, Vaisse C, Reiter JF, and Berbari NF (2023). Physiological Condition-Dependent Changes in Ciliary GPCR Localization in the Brain. eNeuro 10. 10.1523/ENEURO.0360-22.2023.
68. Wiegering A, Dildrop R, Kalfhues L, Spychala A, Kuschel S, Lier JM, Zobel T, Dahmen S, Leu T, Struchtrup A, et al. (2018). Cell type-specific regulation of ciliary transition zone assembly in vertebrates. EMBO J. 37, e97791. 10.15252/embj.201797791. [PubMed: 29650680]
69. Brailov I, Bancila M, Brisorgueil MJ, Miquel MC, Hamon M, and Vergé D (2000). Localization of 5-HT(6) receptors at the plasma membrane of neuronal cilia in the rat brain. Brain Res. 872, 271–275. 10.1016/s0006-8993(00)02519-1. [PubMed: 10924708]
70. Siljee JE, Wang Y, Bernard AA, Ersoy BA, Zhang S, Marley A, Von Zastrow M, Reiter JF, and Vaisse C (2018). Subcellular localization of MC4R with ADCY3 at neuronal primary cilia underlies a common pathway for genetic predisposition to obesity. Nat. Genet. 50, 180–185. 10.1038/s41588-017-0020-9. [PubMed: 29311635]
71. Ortega-Martínez S (2015). A new perspective on the role of the CREB family of transcription factors in memory consolidation via adult hippocampal neurogenesis. Front. Mol. Neurosci. 8, 46. 10.3389/fnmol.2015.00046. [PubMed: 26379491]
72. Mayr B, and Montminy M (2001). Transcriptional regulation by the phosphorylation-dependent factor CREB. Nat. Rev. Mol. Cell Biol. 2, 599–609. 10.1038/35085068. [PubMed: 11483993]
73. Lonze BE, and Ginty DD (2002). Function and regulation of CREB family transcription factors in the nervous system. Neuron 35, 605–623. 10.1016/s0896-6273(02)00828-0. [PubMed: 12194863]
74. Kucharova K, Chang Y, Boor A, Yong VW, and Stallcup WB (2011). Reduced inflammation accompanies diminished myelin damage and repair in the NG2 null mouse spinal cord. J. Neuroinflammation 8, 158. 10.1186/1742-2094-8-158. [PubMed: 22078261]
75. Ventura A, Meissner A, Dillon CP, McManus M, Sharp PA, Van Parijs L, Jaenisch R, and Jacks T (2004). Cre-lox-regulated conditional RNA interference from transgenes. Proc. Natl. Acad. Sci. USA 101, 10380–10385. 10.1073/pnas.0403954101. [PubMed: 15240889]

76. Dobin A, Davis CA, Schlesinger F, Drenkow J, Zaleski C, Jha S, Batut P, Chaisson M, and Gingeras TR (2013). STAR: ultrafast universal RNA-seq aligner. Bioinformatics 29, 15–21. 10.1093/bioinformatics/bts635. [PubMed: 23104886]

77. Love MI, Huber W, and Anders S (2014). Moderated estimation of fold change and dispersion for RNA-seq data with DESeq2. Genome Biol. 15, 550. 10.1186/s13059-014-0550-8. [PubMed: 25516281]

78. Roesch K, Jadhav AP, Trimarchi JM, Stadler MB, Roska B, Sun BB, and Cepko CL (2008). The transcriptome of retinal Müller glial cells. J. Comp. Neurol. 509, 225–238. 10.1002/cne.21730. [PubMed: 18465787]

79. Kang SH, Fukaya M, Yang JK, Rothstein JD, and Bergles DE (2010). NG2+ CNS glial progenitors remain committed to the oligodendrocyte lineage in postnatal life and following neurodegeneration. Neuron 68, 668–681. 10.1016/j.neuron.2010.09.009. [PubMed: 21092857]

80. Srinivas S, Watanabe T, Lin CS, William CM, Tanabe Y, Jessell TM, and Costantini F (2001). Cre reporter strains produced by targeted insertion of EYFP and ECFP into the ROSA26 locus. BMC Dev. Biol. 1, 4. 10.1186/1471-213x-1-4. [PubMed: 11299042]

81. Haycraft CJ, Zhang Q, Song B, Jackson WS, Detloff PJ, Serra R, and Yoder BK (2007). Intraflagellar transport is essential for endochondral bone formation. Development 134, 307–316. 10.1242/dev.02732. [PubMed: 17166921]

82. Mei F, Fancy SPJ, Shen YAA, Niu J, Zhao C, Presley B, Miao E, Lee S, Mayoral SR, Redmond SA, et al. (2014). Micropillar arrays as a high-throughput screening platform for therapeutics in multiple sclerosis. Nat. Med. 20, 954–960. 10.1038/nm.3618. [PubMed: 24997607]

83. Niu J, Tsai HH, Hoi KK, Huang N, Yu G, Kim K, Baranzini SE, Xiao L, Chan JR, and Fancy SPJ (2019). Aberrant oligodendroglialvascular interactions disrupt the blood-brain barrier, triggering CNS inflammation. Nat. Neurosci. 22, 709–718. 10.1038/s41593-019-0369-4. [PubMed: 30988524]

Highlights

- OPCs need primary cilia for proliferation in development and white matter injury
- The primary cilium is not required for canonical Hh signaling in OPCs
- A cAMP/CREB signaling axis initiated within the primary cilium regulates OPC proliferation

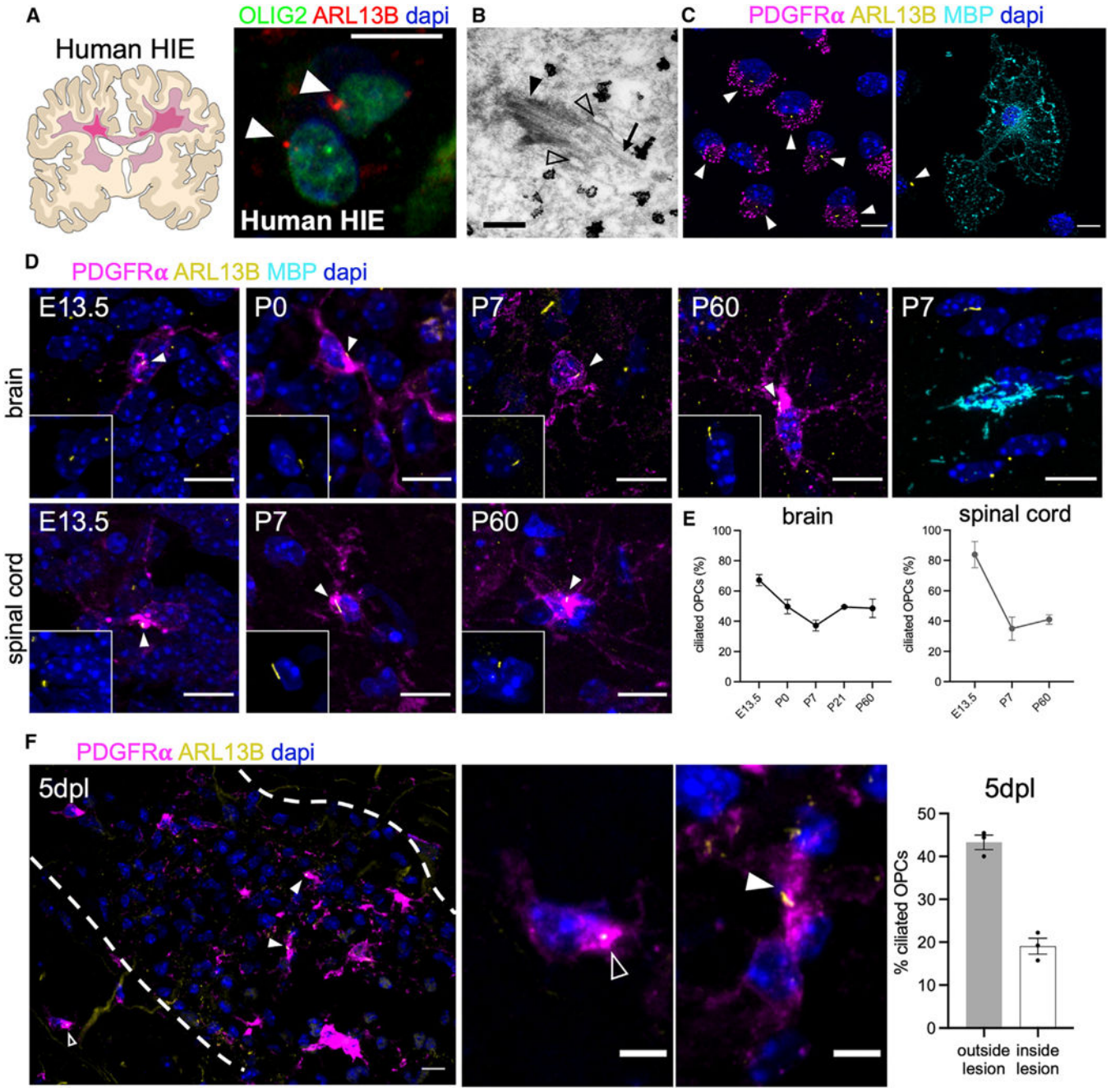

Figure 1. OPCs are dynamically ciliated during development and injury

(A) Immunofluorescence for cilia (Arl13b, red) in OL-lineage cells (Olig2, green) in tissue collected from human HIE. Scale bar, 10 μm.

(B) Electron micrograph of cilia in OPCs labeled with immunogold GFP from P60 NG2-EGFP mice. Scale bar, 200 nm. Black arrows, axoneme; black arrowheads, basal body; empty arrowheads, ciliary pockets.

(C) Immunofluorescence for cilia (Arl13b, yellow) in OPCs (Pdgfrα, magenta) and mature OLs (MBP, cyan) isolated from P7 rats. Arrowheads mark ciliated OPCs. Nuclei are labeled with DAPI. Scale bars, 10 μm.

(D) Immunofluorescence for cilia (Arl13b, yellow) in OPCs (Pdgfrα, magenta) and mature OLs (MBP, cyan) at the indicated time points in the developing mouse brain (top row) and spinal cord (bottom row). Arrowheads mark ciliated OPCs. Nuclei are labeled with DAPI. Scale bars, 10 μm.

(E) Quantification of the percentage of ciliated OPCs over total OPCs across different time points in mouse brain and spinal cord development. n = 4–5 mice per time point.

(F) Immunofluorescence and quantification for cilia (Arl13b, yellow) and OPCs (Pdgfrα, magenta) at 5 dpl with lysolecithin in the adult mouse spinal cord dorsal funiculus. Arrowheads mark ciliated OPCs. Nuclei are labeled with DAPI. Scale bars, 50 μm and 5 μm (inset).

See also Figure S1.

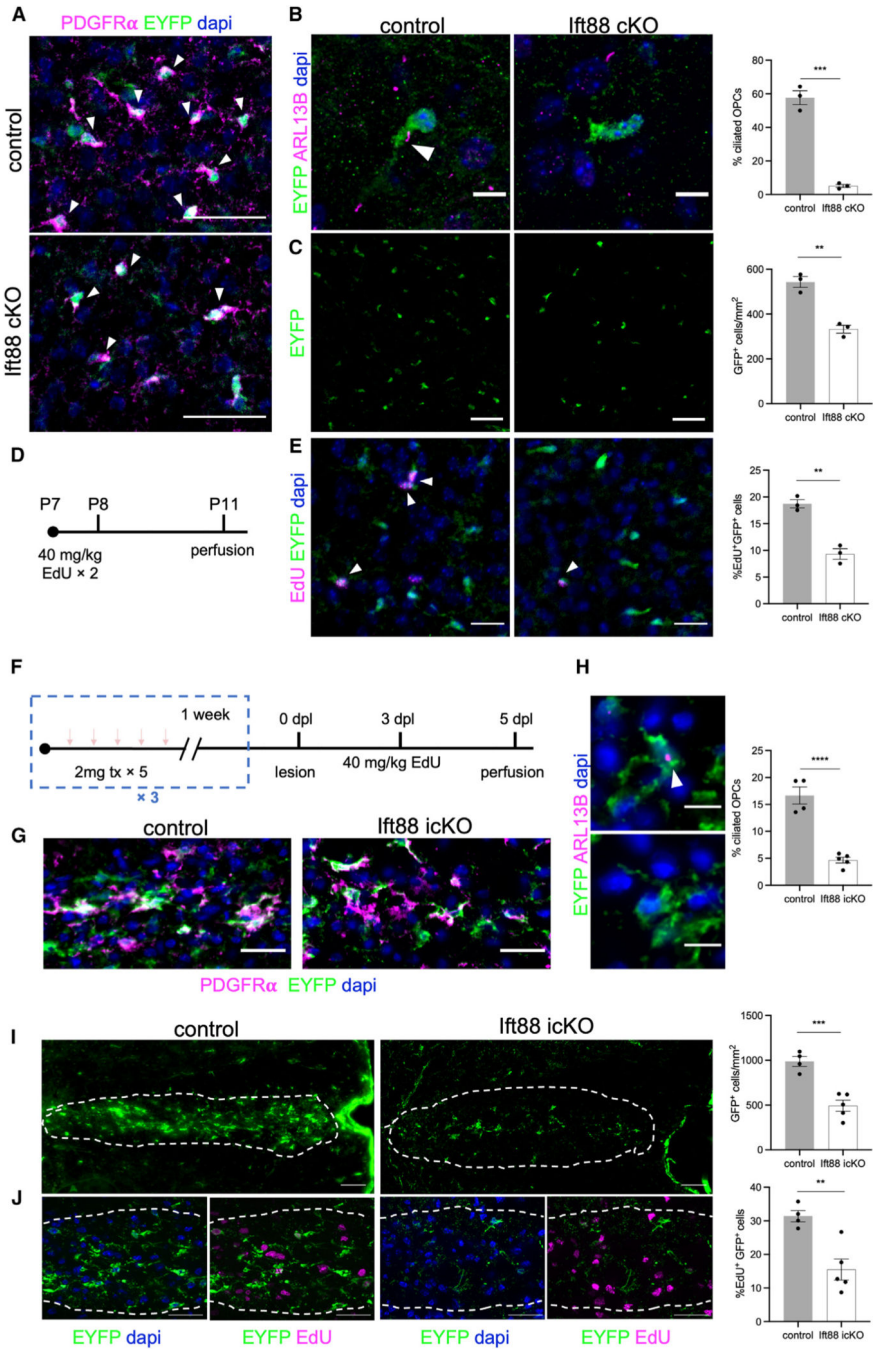

Figure 2. Disruption of ciliogenesis reduces OPC expansion

(A) Detection of EYFP (GFP, green) in OPCs (arrowheads; Pdgfrα, magenta) in P7 Pdgfrα-Cre: Ift88$^{fl/wt}$; RosaEYFP (control) and Pdgfrα-Cre: Ift88$^{fl/fl}$; RosaEYFP (Ift88 cKO) mice. Scale bar, 50 μm.

(B) Detection and quantification of cilia (Arl13b, magenta) in oligodendroglia (EYFP, green) from control and Ift88 cKO mice. n = 3 mice per genotype. Data are represented as mean ± SEM. Scale bar, 10 μm.

(C) Representative images of recombined oligodendroglia (EYFP, green) in the cortex of control and Ift88 cKO mice at P7. Scale bar, 50 μm. Also shown is quantification of $EYFP^+$ oligodendroglial density (calculated per mm^2) in the cortex of control and Ift88 cKO mice at P7. n = 3 mice per genotype. p = 0.0021. Difference between means −211.2 ± 29.97. 95% confidence interval −294.4 to −127.9.

(D) Experimental paradigm for EdU injections in the developing mouse cortex.

(E) Representative images of EdU (magenta) and oligodendroglia (EYFP, green) in the cortex of control and Ift88 cKO animals, with arrows indicating colocalized EdU^+EYFP^+ cells. Scale bar, 25 μm. Also shown is quantification of GFP^+ oligodendroglia that are EdU^+, calculated by percentage of EdU^+EYFP^+ (EdU, magenta; GFP, green) cells over total $EYFP^+$ cells at P11. n = 3 mice per genotype.

(F) Experimental paradigm for tamoxifen injections and lysolecithin lesions in Pdgfrα-CreERT: $Ift88^{fl/fl}$; RosaEYFP (Ift88 icKO) and control mice.

(G) Detection of EYFP (green) in OPCs (arrowheads; Pdgfrα, magenta) in dorsal funiculus lysolecithin lesions at 5 dpl in control and Ift88 icKO mice. Scale bar, 25 μm.

(H) Detection and quantification of cilia (Arl13b, magenta) in oligodendroglia (EYFP, green) within lesions from control and Ift88 icKO mice at 5 dpl. Scale bar, 10 μm.

(I) Representative images of recombined OPCs (EYFP, green) in dorsal funiculus lesions 5 dpl from control and Ift88 icKO mice. Scale bars, 50 μm. Also shown is quantification of $EYFP^+$ oligodendroglia density (calculated per mm^2) in 5 dpl dorsal funiculus. n = 4–5 mice per genotype. p = 0.0007. Difference between means −495.1 ± 85.26. 95% confidence interval −696.7 to −293.5.

(J) Representative images of $EYFP^+EdU^+$ proliferating oligodendroglia within lesions at 5 dpl from control and Ift88 icKO mice. Scale bars, 50 μm. Also shown is quantification of $EYFP^+$ oligodendroglia that are EdU^+, calculated by percentage of EdU^+EYFP^+ (EdU, magenta; EYFP, green) cells over total $EYFP^+$ cells in 5 dpl dorsal funiculus. n = 4–5 mice per genotype.

For (C)–(J), significance was determined via unpaired t tests. A p value less than 0.05 was considered statistically significant, with significance denoted as follows: **p < 0.01, ***p < 0.001, ****p < 0.0001. Data are represented as mean ± SEM. See also Figures S2–S4.

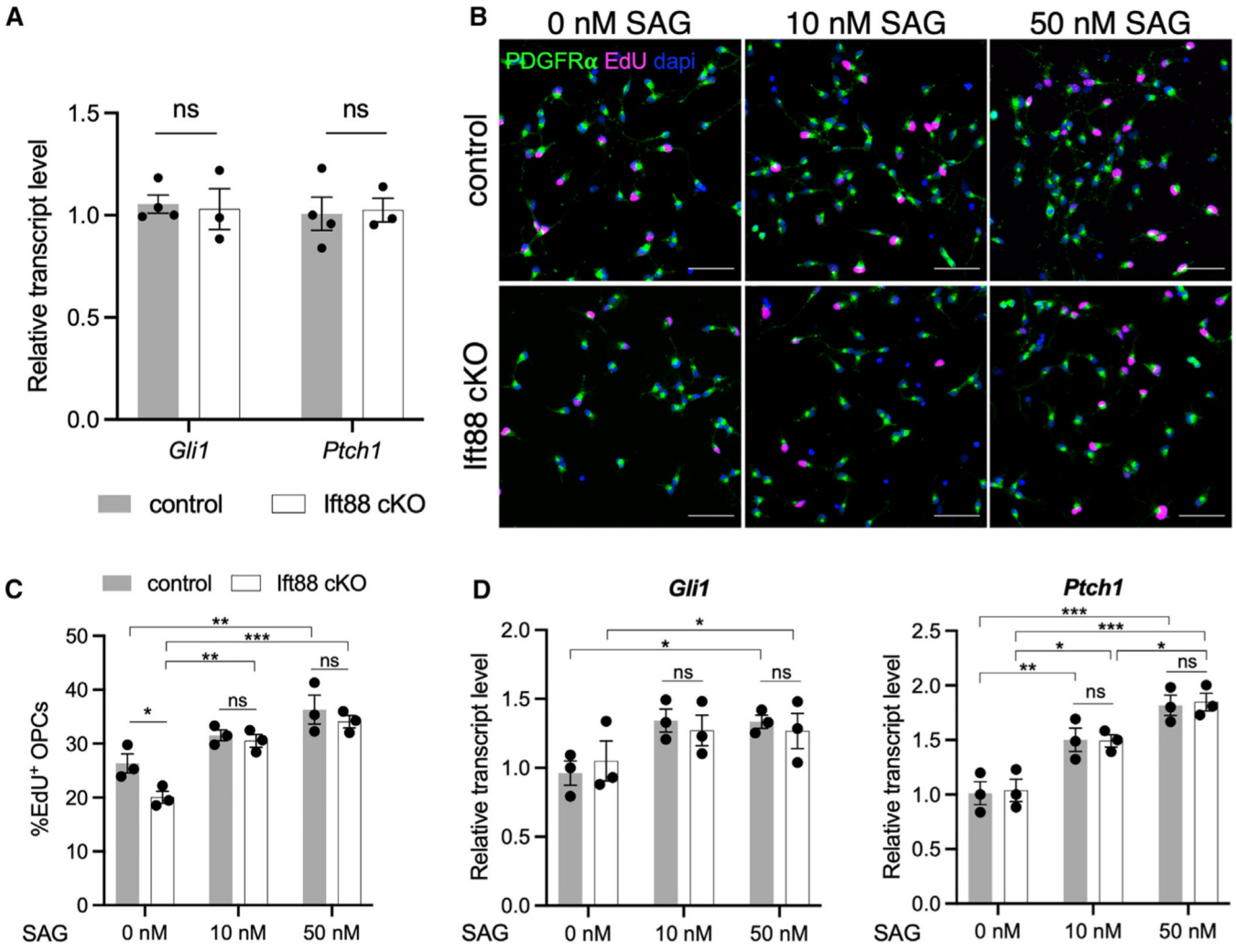

Figure 3. Hh activity is unaffected by the loss of OPC cilia *in vitro*

(A) qRT-PCR of Gli1 and Ptch1 transcripts shows no difference in expression between OPCs isolated from P7 control and Ift88 cKO mice. n = 3 mice per genotype.

(B) 10 nM and 50 nM of SAG promotes proliferation in control and Ift88 cKO OPCs *in vitro*. Scale bars, 50 μm.

(C) Quantification of $EdU^+Pdgfr\alpha^+$ (EdU, magenta; Pdgfrα, green) proliferating OPCs, calculated by percentage of $EdU^+Pdgfr\alpha^+$ cells over total $Pdgfr\alpha^+$ cells. n = 3 mice per genotype.

(D) qRT-PCR of Gli1 and Ptch1 transcripts in OPCs after treatment with 10 nM and 50 nM SAG. n = 3 mice per genotype.

For (C) and (D), significance was determined via two-way ANOVA with Tukey's post hoc analysis. A p value less than 0.05 was considered statistically significant, with significance denoted as follows: ns, not significant; *p < 0.05, **p < 0.01, ***p < 0.001, ****p < 0.0001. Data are represented as mean ± SEM. See also Figure S5.

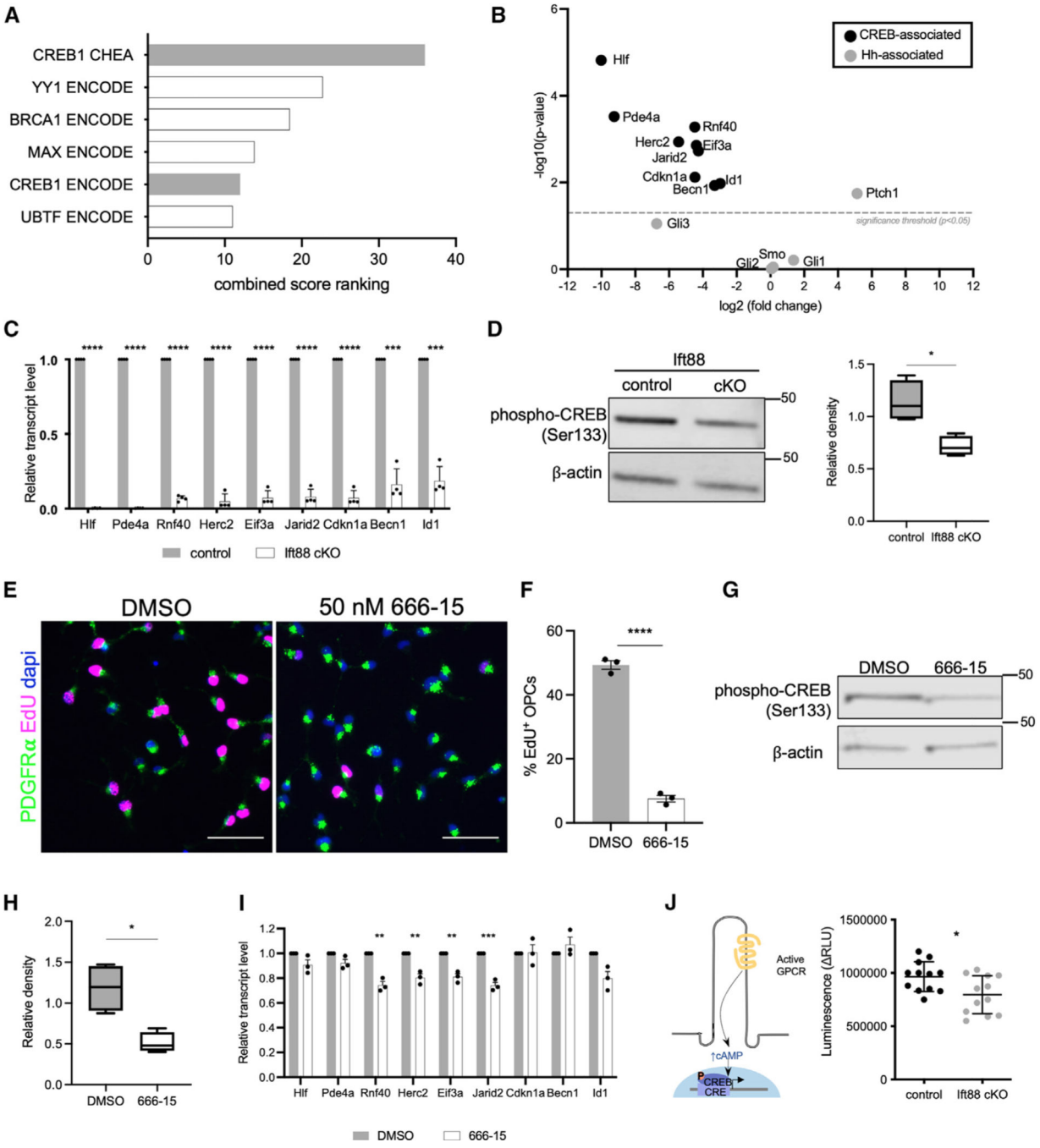

Figure 4. OPC cilia regulate CREB activity to promote OPC proliferation

(A) Graphed combined score rankings from Enrichr, comparing downregulated genes identified from RNA-seq in Ift88 cKO with control OPCs.

(B) CREB1-associated genes and Hh-associated genes plotted by fold change and significance. Significance threshold was set as $p < 0.05$.

(C) qRT-PCR analysis of Ift88 cKO and control OPCs for CREB1-associated genes identified in Figure 1B. Transcript levels in Ift88 cKO are depicted relative to controls. n = 4 per genotype. Significance was determined via unpaired t tests. A p value less than

0.05 was considered statistically significant, with significance denoted as follows: ***p < 0.001 and ****p < 0.0001. Data are represented as mean ± SEM.

(D) Western blot for pCREB in control and Ift88 cKO OPCs. Quantification of the western blot shows pCREB expression in Ift88 cKO relative to controls and is represented as a box-and-whisker plot depicting minima, maxima, median, and interquartile range.

(E) P7 WT rat OPCs (Pdgfrα, green) treated with the CREB inhibitor 666–15 and labeled with EdU (magenta). Scale bar, 50 μm.

(F) Quantification of OPCs that are EdU^+ in cultures treated with 50 nM 666–15 versus DMSO control, calculated by percentage of $EdU^+Pdgfr\alpha^+$ cells over total $Pdgfr\alpha^+$ cells. n = 3 per condition. Significance was determined via unpaired t test; p < 0.0001. Data are represented as mean ± SEM.

(G) Western blot for pCREB from proteins isolated from WT OPCs treated with 50 nM 666–15 or DMSO control.

(H) Quantification of the immunoblot from (G). pCREB expression in 666–15-treated OPCs is shown relative to that of DMSO-treated OPCs. Data are represented as a box-and-whisker plot depicting minima, maxima, median, and interquartile range.

(I) Relative transcript levels from qRT-PCR of CREB1-associated genes identified in RNA-seq studies from OPCs treated with 666–15 or DMSO; 666–15 reduces expression of CREB1-associated genes identified in RNA-seq studies. Transcript levels in 666–15 cultures are depicted relative to controls. n = 3 per condition.

Significance was determined via unpaired t tests. A p value less than 0.05 was considered statistically significant, with significance denoted as follows: **p < 0.005 and ***p < 0.001. Data are represented as mean ± SEM.

(J) cAMP levels in Ift88 cKO OPCs compared with controls assessed via cAMP Glo assay. n = 12 per genotype. Unpaired t test, p < 0.05; data are represented as mean ± SEM.

For (D) and (H), statistical significance was determined via unpaired t test. A p value less than 0.05 was considered statistically significant, with significance denoted as follows: *p < 0.05. See also Figure S6.

KEY RESOURCES TABLE

REAGENT or RESOURCE	SOURCE	IDENTIFIER
Antibodies		
Rabbit anti-ARL13B	Proteintech	Cat#17711–1-AP; RRID:AB_2060867
Mouse anti-ARL13B	UC Davis/NIH Neuromab Facility	Cat# 73–287; RRID:AB_11000053
Rat anti-Pdgfra	BD Biosciences	Cat# 558774; RRID:AB_397117
Rabbit anti-Pdgfra	Gift from W. Stallcup	Kucharova et al., 2011[74]
Rabbit anti-Olig2	Millipore	Cat# AB9610; RRID:AB_570666
Mouse anti-Olig2	Millipore	Cat# MABN50; RRID:AB_10807410
Mouse anti-CC1	Millipore	Cat# OP80; RRID:AB_2057371
Rat anti-MBP	Bio-Rad	Cat# MCA409S; RRID:AB_325004
Chicken anti-GFP	Aves	Cat# GFP-1020; RRID:AB_10000240
Rabbit anti-GFP	Thermo Fisher	Cat# G10362; RRID:AB_2536526
Rabbit anti-cleaved caspase-3	Cell Signaling Technology	Cat# 9661; RRID:AB_2341188
Rabbit anti-phospho-CREB	Cell Signaling Technology	Cat# 9198; RRID:AB_2561044
Rabbit anti-β-actin	Proteintech	Cat# 20536–1-AP; RRID:AB_10700003
Rabbit anti-IFT88	Proteintech	Cat # 13967–1-AP; RRID:AB_2121979
Biological samples		
Human newborn HIE tissue	UCSF Pediatric Neuropathology Research Laboratory (PNRL)	https://pediatrics.ucsf.edu/neonatology/newborn-brain-research-institute
Chemicals peptides and recombinant proteins		
Tamoxifen	Sigma-Aldrich	Cat# T5648
Lysolecithin	Sigma-Aldrich	Cat# L4129
Human recombinant PDGF-AA	PeproTech	Cat# 100–13A
Smoothened Agonist	Milllipore	Cat# 566660
666–15	MedChemExpress	Cat# HY-101120
DMSO	Sigma-Aldrich	Cat# D8418
Critical commercial assays		

REAGENT or RESOURCE	SOURCE	IDENTIFIER
RNAeasy Mini Kit	QIAGEN	Cat# 74104
iSCRIPT cDNA Synthesis Kit	Bio-Rad	Cat# 1708891
cAMP-Glo	Promega	Cat# V1501
Deposited data		
RNA-sequencing of control versus Ift88 cKO OPCs at P11	Gene Expression Omnibus	GSE243997
Experimental models: Organisms/strains		
Mouse: Ift88 fl/fl *Ift88^{tm1Bky}*	The Jackson Laboratory	Stock No. 022409; RRID:IMSR_JAX:022409
Mouse: Pdgfra-CreERT *Tg(Pdgfra-cre/ERT)467Dbe*	The Jackson Laboratory	Stock No. 018280; RRID:IMSR_JAX:018280
Mouse: Pdgfra-Cre *Tg(Pdgfra-Cre)1Clc/J*	The Jackson Laboratory	Stock No. 013148; RRID:IMSR_JAX:01314
Mouse: RosaEYFP (R26R-EYFP) *Gt(ROSA)26Sor$^{tm1(EYFP)Cos}$*	The Jackson Laboratory	Stock No. 006148; RRID:IMSR_JAX:006148
Oligonucleotides		
Ift88 flox genotyping primer F: AGGGAAGGGACTTAGGAATGA R: GACCACCTTTTTAGCCTCCTG	Integrated DNA Technologies	N/A
RosaEYFP genotyping primers WT F: CTGGCTTCTGAGGACCG WT R: CAGGACAACGCCCACACA GFP F: AGGGCGAGGAGCTGTTCA GFP R: TGAAGTCGATGCCCTTCAG	Integrated DNA Technologies	N/A
See Table S1 for qPCR primer sequences		N/A
Recombinant DNA		
pSiCoR	(Ventura et al.)[75]	Gift from Tyler Jacks, RRID:Addgene_11579
pSiCoR-shEif3a-EGFP target sequence: GCCTCAGTTGATGGCAAATTA	This paper	TRC clone ID: TRCN0000309153
pSiCoR-shJarid2-EGFP target sequence: TGCCCAACAGTATGGTATATT	This paper	TRC clone ID: TRCN0000234444
pSiCoR-shCdkn1a-EGFP target sequence: GACCAGCCTGACAGATTTCTA	This paper	TRC clone ID: TRCN0000042584

Cell Rep. Author manuscript; available in PMC 2023 December 12.

REAGENT or RESOURCE	SOURCE	IDENTIFIER
psPAX2	Unpublished from Didier Trono lab	Gift from Didier Trono, RRID:Addgene_12260
pMD2.G	Unpublished from Didier Trono lab	Gift from Didier Trono, RRID:Addgene_12259
Software and algorithms		
GraphPad Prism 9	GraphPad Software	https://www.graphpad.com/scientific-software/prism/; RRID:SCR_015807
Fiji	Open Source	https://fiji.sc/; RRID:SCR_002285
ZEN Digital Imaging for Light Microscopy	Zeiss	RRID:SCR_013672
STAR	(Dobin et al.)[76]	https://github.com/alexdobin/STAR/releases; RRID:SCR_004463
DESeq2	(Love et al.)[77]	http://www.bioconductor.org/packages/release/bioc/html/DESeq2.html; RRID:SCR_015687